AGU PUBLICATIONS

JGR

Journal of Geophysical Research: Solid Earth

RESEARCH ARTICLE
10.1002/2016JB012884

Key Points:
- Model for 3-D crustal velocities derived for U.S. and Canada from repeated geodetic data
- NA_ICE-6G reference frame introduced to minimize velocities in "stable" North American plate after removing GIA effects
- Uplift rates exceed 30 mm/yr in southeastern Alaska due to modern-day deglaciation

Supporting Information:
- Supporting Information S1
- Data Set S1
- Data Set S2
- Software S1

Correspondence to:
R. A. Snay,
rssnay@aol.com

Citation:
Snay, R. A., J. T. Freymueller, M. R. Craymer, C. F. Pearson, and J. Saleh (2016), Modeling 3-D crustal velocities in the United States and Canada, *J. Geophys. Res. Solid Earth*, *121*, 5365–5388, doi:10.1002/2016JB012884.

Received 4 FEB 2016
Accepted 8 JUN 2016
Accepted article online 12 JUN 2016
Published online 15 JUL 2016

Modeling 3-D crustal velocities in the United States and Canada

Richard A. Snay[1], Jeffrey T. Freymueller[2], Michael R. Craymer[3], Chris F. Pearson[4], and Jarir Saleh[5]

[1]National Geodetic Survey (retired), Montgomery Village, Maryland, USA, [2]Geophysical Institute, University of Alaska Fairbanks, Fairbanks, Alaska, USA, [3]Geodetic Survey Division, Natural Resources Canada, Ottawa, Ontario, Canada, [4]Surveying Department, University of Otago, Dunedin, New Zealand, [5]National Geodetic Survey, Silver Spring, Maryland, USA

Abstract A numerical model for three-dimensional (3-D) crustal velocities has been derived for most of the United States and Canada, primarily from repeated geodetic data. This model provides a foundation for a prototype of the TRANS4D software. TRANS4D is being developed to enable geospatial professionals and others to transform 3-D positional coordinates across time. The derived model reveals several macroscopic features of the 3-D velocity field, including the pervasive presence of the glacial isostatic adjustment associated with the past melting of the ice fields that formed more than 19,000 years ago during the Last Glacial Maximum. In this study, the present-day 3-D velocity field associated with this melting (as estimated via the recently published ICE-6G_C (VM5a) model) was subtracted from this study's total 3-D velocity field to identify features of the residual velocity field. In particular, this study introduces the NA_ICE-6G reference frame in which residual horizontal velocities have magnitudes that are less than 2 mm/yr everywhere east of longitude 104°W and south of latitude 60°N, except in southern Texas. Residual horizontal velocities of greater magnitude are found west and/or north of these two boundaries, and they are due mostly to interactions among tectonic plates with localized pockets due to other geophysical phenomena. Large residual vertical velocities, some with values exceeding 30 mm/yr, are found in southeastern Alaska. The uplift occurring here is due to present-day melting of glaciers and ice fields formed during the Little Ice Age glacial advance that occurred between 1550 A.D. and 1850 A.D.

1. Introduction

A numerical model for three-dimensional (3-D) crustal velocities as a function of latitude and longitude has been developed for the conterminous United States (CONUS) and for most of Alaska and Canada. This model has been derived primarily from repeated geodetic observations performed, either continuously or episodically, at approximately 4300 sites. The repeated geodetic data correspond to time series of values that have been edited to remove the effects of coseismic and transient motion as best as possible. Each time series is then applied to obtain an average rate of change of a geodetic quantity over the time span of the corresponding data. The quantity is usually a component of 3-D positional coordinates, but it can also be the distance between two points. Sometimes the computation of this rate involved solving for parameters that characterize periodic motion. Nevertheless, the output of interest is the average rate of change of the geodetic quantity being measured. Thus, the 3-D crustal velocities, produced in this study, represent average velocities over the past few decades.

The horizontal velocity field is more complete than previous studies but is generally similar to that of past compilations in most areas; the vertical velocity field presented here is new. Here the vertical velocity at a location is oriented normal to the geocentric ellipsoid whose size and shape equal those adopted for the Geodetic Reference System of 1980 [*Moritz*, 1984]. A positive vertical velocity corresponds to motion away from Earth's center of mass.

This new 3-D velocity model provides a foundation for a prototype of the TRANS4D software package, where TRANS4D is short for "Transformations in Four Dimensions." TRANS4D is being developed to enable geospatial professionals and others to transform 3-D positional coordinates across time and between spatial reference frames. In particular, TRANS4D incorporates 4-D transformations among all currently existing realizations of the International Terrestrial Reference System, all currently existing realizations of the World Geodetic System of 1984, and several recent realizations of the North American Datum of 1983. Fortran90 source code for Version 0.1 of TRANS4D, together with a *Users Guide*, may be found among the supporting

information associated with this publication. TRANS4D has been designed to expand upon the scope of the Horizontal Time-Dependent Positioning (HTDP) software [*Pearson and Snay*, 2014; *Pearson et al*., 2014; *Snay et al*., 2013; *Pearson and Snay*, 2013; *Pearson et al*., 2010; *Snay and Pearson*, 2010; *Pearson and Snay*, 2007; *Snay*, 1999]. HTDP incorporates models for horizontal crustal motion only and enables its users to transform horizontal positional coordinates across time and between spatial reference frames. Users can apply the HTDP software interactively on the Web at geodesy.noaa.gov/TOOLS/Htdp/Htdp.shtml. In addition to addressing velocities in all three spatial dimensions, TRANS4D improves upon HTDP by also providing (1) velocities for much of Canada and (2) standard deviations for its estimated velocities.

The first version of HTDP was released in 1992. Unfortunately, many of the early HTDP versions incorporated rather crude crustal motion models, because the early models were based on a relatively small amount of triangulation/trilateration data. However, HTDP gradually evolved to its current level of sophistication as more precise geodetic data, especially GPS data, became available and as the scientific understanding of horizontal crustal motion matured. With TRANS4D, a similar evolution of its current crustal motion models is anticipated to occur over a period of several years. The understanding of vertical crustal motion is currently limited, because many studies have focused on horizontal motions due to their greater signal-to-noise ratio. Vertical motions can be caused by a combination of tectonics; glacial isostatic adjustment (GIA, also sometimes called postglacial rebound); surface loading due to changing hydrologic, cryospheric, or atmospheric loads; changes in groundwater and aquifer pressure; and volcanic activity. GPS-derived vertical positions are also subject to larger uncertainties and more potential for systematic errors than GPS-derived horizontal positions. In addition, modeling vertical crustal motion is more complex than modeling horizontal crustal motion due to (1) more ubiquitous occurrence of significant spatial variability over short distances (rates of vertical motion often differ significantly between locations less than 1 km apart); (2) more ubiquitous occurrence of significant temporal variability (rates of vertical motion can change over time due to both natural phenomena and anthropogenic (human) activities, such as groundwater withdrawal); and (3) dependence of measured vertical motion on the depth to which each geodetic reference station is anchored (due to possible compaction within Earth's shallower layers and hydrologic cycles within aquifers).

The third item is especially troublesome because most (but not all) geodetic reference stations are anchored deep enough to avoid the fluctuations in vertical motion, which occur within Earth's shallower layers. Many people, however, are concerned with the hazards associated with flooding, whereupon these people place greater importance on the vertical motion occurring at Earth's surface rather than that occurring at depth. Unfortunately, TRANS4D's model pertains more relevantly to deep vertical motion. In view of the above three items, the development of accurate vertical motion models will necessarily depend on data types other than those used in this study, for example, remote sensing data.

Section 2 of this paper provides an overview of the TRANS4D software, and section 3 discusses the geodetic data used to develop the velocity models. Section 4 and its subsections describe the various processes employed to produce the models. Sections 5 and 6 present the horizontal and vertical components, respectively, of the newly developed velocity model and discuss some geophysical results revealed by this model. Section 7 presents standard deviations for the model-generated velocities.

2. TRANS4D Overview

TRANS4D enables its users to perform each of the following functions: (1) obtain estimates for 3-D crustal velocities, (2) obtain estimates for 3-D crustal displacements between two dates, (3) transform 3-D positional coordinates from one reference frame to another and/or from one date to another, (4) transform certain types of geodetic observations from one reference frame to another and/or from one date to another, and (5) transform 3-D crustal velocities from one reference frame to another.

TRANS4D's *Users Guide* (contained in the Supporting Information S1) provides details as to how TRANS4D performs these five functions. To support its capabilities, TRANS4D incorporates numerical models for 3-D crustal velocity, as well as models for the motion associated with 29 earthquakes (most with moment magnitude > 6) and a separate model for the postseismic motion associated with the *M*7.9 Denali Fault earthquake that occurred in central Alaska on 3 November 2002. This paper focuses on the nature and development of only the 3-D crustal velocity models. The *Users Guide* cites publications describing TRANS4D's models for coseismic and postseismic motion. The velocity model includes the 3-D motion associated with

GIA, as long as it is steady in time (over the past decade or so). This is generally the case except in areas, such as Alaska, which are undergoing active deglaciation that can produce temporal variations in crustal velocities. Seasonal and interannual hydrologic loading variations can produce both periodic motion and variations in vertical motion rates [e.g., *Fu et al*., 2012; *Amos et al*., 2014; *Argus et al*., 2014a; *Borsa et al*., 2014; *Fu et al*., 2015]. TRANS4D does not yet include models for such periodic motion, nor does it include models for transient motion (such as that associated with slow earthquakes).

3. Geodetic Data

The 3-D velocity model contained in TRANS4D (Version 0.1) has been formulated by using 3-D velocity vectors derived from repeated GPS observations, repeated trilateration observations, and repeated very-long-baseline-interferometry (VLBI) observations at more than 4300 geodetic-quality reference stations. These geodetically derived velocity vectors were obtained from seven separate solutions. In many cases, a velocity vector found in one solution may have been computed from essentially the same geodetic data used to compute a velocity vector found in another solution. The seven solutions include the following:

The International GNSS Service (IGS) cumulative solution based on continuous GPS data observed through week 36 of 2013 (GPS Week 1756) at IGS-affiliated stations distributed around the world (ftp://cddis.gsfc.nasa.gov/gps/products). The IGS updates its solution on a weekly basis. The IGS solution is based on time series of GPS-derived positional coordinates that have been created collaboratively by several institutions. The IGS produces positional coordinates and velocities that are referred to the IGS08 reference frame [*Rebischung et al*., 2012]. IGS08 represents a GPS-based realization of the International Terrestrial Reference Frame of 2008 (ITRF2008) [*Altamimi et al*., 2011]. The IGS considers IGS08 velocities to be essentially equivalent to ITRF2008 velocities in the sense that there are no known systematic differences between these two sets of velocities. Recently, the IGS adopted the IGb08 reference frame, whose velocities are also considered to be essentially equivalent to ITRF2008 velocities.

The U.S. National Geodetic Survey (NGS) solution released on 6 September 2011 [*Griffiths et al*., 2010]. This solution provides estimated IGS08-consistent velocities for continuous GPS stations contained in the NGS-affiliated Continuously Operating Reference Station (CORS) network (geodesy.noaa.gov/CORS/), as well as most of the IGS-affiliated continuous GPS stations distributed around the world.

The Natural Resources Canada (NRCan) solution for IGS08-consistent velocities at both continuous and episodically monitored GPS stations located in and around Canada [*Craymer et al*., 2011].

The MEASURES (Making Earth System Data Records for Use in Research Environments) solution that the Jet Propulsion Laboratory and Scripps Orbit and Permanent Array Center jointly released in June 2013 [*Bock and Webb*, 2012]. This solution provides estimated IGS08-consistent velocities for continuous GPS stations contained in the Plate Boundary Observatory (pboweb.unavco.org), as well as many other continuous GPS stations distributed around the world.

The solution published by McCaffrey et al. [2013] *which provides velocities for many continuous GPS stations, as well as for many episodically monitored GPS stations, located mainly in and around northwestern CONUS*. McCaffrey et al. aligned their velocities to the SNARF 2.0 reference frame, which is designed to provide horizontal velocities relative to "stable" North America [*Herring et al*., 2008].

The Southern California Earthquake Center (SCEC) solution known as "Crustal Motion Model Four" [*Shen et al*., 2011] *which provides estimated velocities for continuous GPS stations, as well as for episodically monitored GPS stations, located mainly in and around southern California*. This solution also provides estimated velocities derived from trilateration data observed in California under the auspices of the U.S. Geological Survey and from VLBI data observed under the auspices of NASA. Shen et al. aligned their velocities to the SNARF 1.0 reference frame, which is also designed to provide velocities relative to "stable" North America [*Blewitt et al*., 2005].

A solution produced by the University of Alaska Fairbanks (UAF) which provides estimated IGS08-consistent velocities for continuous GPS stations and episodically monitored GPS stations located in and around Alaska.

Using the combination process described in Appendix A, the geodetically derived velocities from these seven solutions were used to estimate a single 3-D IGS08 velocity for each of the 4925 unique stations

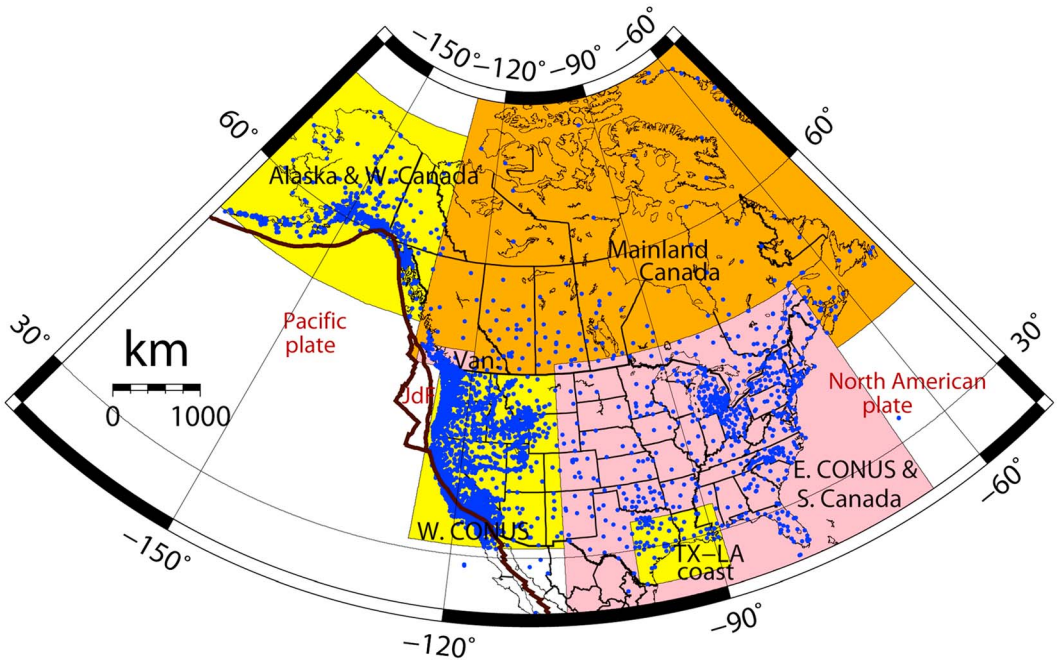

Figure 1. Shaded polygonal areas identify six regions for which 3-D crustal velocity models have been developed. The name of each region appears in black, where Vancouver is abbreviated as "Van." Blue dots identify locations at which 3-D velocities have been derived from repeated geodetic observations. Dark brown line segments denote plate boundaries. Plate names appear in brown, where Juan de Fuca is abbreviated as "JdF".

contained in one or more of the seven solutions. Of these 4925 stations, approximately 4300 of them are located in and around the United States and Canada. The remaining stations span the globe.

In this paper, the velocity estimates contained in the seven solutions are referred to as "stage-1" velocities, and the velocity estimates produced via the combination process are referred to as "stage-2" velocities. In the next section of this paper, a process to model the stage-2 velocities is described. The resulting models provide 3-D velocity estimates as a function of latitude and longitude. These modeled velocities are referred to as "stage-3" velocities in this paper. Stage-3 velocities correspond to the velocities yielded by the TRANS4D software.

For the approximate geographic area of this study, Figure 1 shows the spatial distribution of the approximately 4300 geodetic stations that have derived velocity vectors contained in one or more of the seven solutions. The supporting information (Data Set S1) contains estimated IGS08 stage-2 velocities for these geodetic stations, together with their assigned standard deviations. These standard deviations were not derived via the combination process. Instead, the standard deviation that was assigned to the estimated IGS08 stage-2 velocity component of a station equals the minimum value of the reported standard deviations, pertaining to this velocity component, among all of the stage-1 velocities at this station. This standard deviation was assigned because the various stage-1 velocities for a station are based upon very similar sets of geodetic data and thus do not represent independent estimates.

Table 1. Attributes of the Modeled Regions

Region	Latitude Extent	Longitude Extent	Grid Spacing
West CONUS	31°N–49°N	107°W–125°W	0.25°
Texas-Louisiana Coast	26°N–33°N	89°W–99°W	0.25°
East CONUS and South Canada	24°N–50°N	66°W–107°W	0.5°
Vancouver	49°N–51°N	120°W–129°W	0.25°
Alaska and West Canada	53°N–73°N	130°W–170°W	0.25°
Mainland Canada	42°N–78°N	52°W–130°W	1° (lat) 1.5°(lon)

4. Modeling Process Overview

In TRANS4D (Version 0.1), the 3-D velocity model for CONUS, and parts of Alaska and Canada, corresponds to a composite of six separate models, one for each of the six rectangular-shaped regions displayed in Figure 1. The geographic extent of each of these six regions was selected on the basis of the region's data density and the expected spatial variability of the region's velocity field. For each of the six regions, the DYNAP-G software was applied to estimate 3-D IGS08 velocities at the nodes of a regularly spaced 2-D grid in latitude and longitude from the IGS08 stage-2 velocities via a least squares process that uses bilinear interpolation in reverse [*Snay et al*., 1996, 2013]. Table 1 lists each of the six regions together with the attributes of its associated grid.

Because the solution for each region involved estimating 3-D velocities at many more grid nodes than the available number of observed velocities in that region, some grid cells contain few or none of the observed velocity vectors (especially the grid cells located in oceanic areas). For example, the West CONUS (WCONUS) region contains 7373 grid nodes but only 3237 observed velocity vectors. The observed velocity information was thus supplemented with quasi-observations which stipulate that—in each of the three dimensions: north, east, and up—the estimated velocity at a given grid node should approximate the weighted mean of the estimated velocity vectors at its neighboring nodes. The mathematical formulation for these quasi-observations is given as equation (7) in [*Snay et al*., 2013]. Hence, for each grid node, three quasi-observations were introduced, each with an assigned standard deviation. The values of the assigned standard deviations were the same from node to node, but they differed from dimension to dimension. The magnitudes of the assigned standard deviations essentially control the degree of smoothing in each dimension, i.e., the smaller the standard deviation, the smoother the resulting velocity field would be. The assigned standard deviations were computed via an iterative process. After performing a preliminary solution with some trial standard deviations for the quasi-observations, refined standard deviations were computed for the quasi-observations so that the sum of the squares of the weighted residuals (including both the residuals to the true observations and the residuals to the quasi-observations) divided by the solution's degrees of freedom would equal 1 when using the refined standard deviations for the quasi-observations in the final solution.

Note that some regions overlap others. In each overlapping area, the velocity of the composite model equals the velocity of the topmost regional model in accordance with the order that the regions are listed in Table 1. For example, velocity estimates for the Texas-Louisiana Coast region supersede velocity estimates for the East CONUS and South Canada region at all locations where these two regions overlap. Artificial velocities constraints were sometimes introduced at selected grid nodes located along regional boundaries so as to minimize discontinuities across these boundaries.

With the exception of the West CONUS (WCONUS) region and the Alaska and West Canada (AK&WCan) region, the 3-D velocity field of each region was estimated directly from the stage-2 velocities. The WCONUS region and the AK&WCan region needed to be treated differently because the use of DYNAP-G is based on the assumption that 3-D velocities vary somewhat smoothly as a function of latitude and longitude. The velocity fields in WCONUS and AK&WCan fail this assumption because these two regions encompass active fault systems near the margins of the Pacific, North American, and/or Juan de Fuca plates (see Figure 1). A velocity field can vary greatly (even discontinuously) across an active fault. (In this paper, the name "Juan de Fuca" serves as a collective term representing three small tectonic plates of which the Juan de Fuca plate is the largest. The other two plates include the Gorda plate, located immediately south of the Juan de Fuca plate, and the Explorer plate located immediately north of the Juan de Fuca plate.)

Section 4.1 describes the special modeling process used for WCONUS, and section 4.2 describes the special modeling process used for AK&WCan. In section 4.3, the spatial resolution of TRANS4D's velocity model is discussed. Section 4.4 addresses the methods used for dealing with discrepant velocities.

4.1. Modeling Process Used in West CONUS

In the case of WCONUS, Robert McCaffrey and Chris Pearson previously developed a geophysical model for its horizontal velocity field [*Pearson et al*., 2010; *Pearson and Snay*, 2013]. These two scientists used the DEFNODE software [*McCaffrey*, 1995, 2002] for which the region's crust is represented by a network of blocks separated by geologic faults. DEFNODE can apply geodetically derived velocities (and other data) to estimate a Euler pole for each block (which defines the overall horizontal motion of each block across Earth's surface) together with a horizontal strain rate tensor for each block and a slip rate (below a specified depth) for each of several

specified fault segments located along the block boundaries. McCaffrey and Pearson also used 170 fault slip rates and 258 fault slip vector azimuths as data to develop their block fault model for the WCONUS region. McCaffrey and Pearson's latest horizontal velocity model for WCONUS has been encoded into HTDP (Version 3.2). This software was used to yield an IGS08 3-D velocity for each geodetic station, located in WCONUS, at which a stage-2 velocity is also available. (Note that HTDP supplies an estimate of 0.0 mm/yr for the IGS08 vertical velocity of any location.) IGS08 velocity differences, obtained by subtracting the HTDP-generated velocities from their corresponding stage-2 velocities, were then employed (via the DYNAP-G software) to estimate a 3-D velocity difference at each node of a 0.25°-by-0.25° grid spanning WCONUS. The resulting IGS08 3-D velocity difference field was then added to the IGS08 3-D velocity field, encoded into HTDP, to provide a refined IGS08 3-D velocity field for WCONUS. This process effectively circumvents the problem associated with fault-related spatial variability in the horizontal dimensions but not so for the vertical dimension. However, the tectonic vertical velocities in WCONUS are small enough that their variability is easily accounted for in the fit using DYNAP-G.

In addition to the six regions identified in Table 1, TRANS4D includes four other regions (San Andreas, Southern California, Northern California, and Pacific Northwest), each of which resides within the boundary of the West CONUS region. Each of these four regions is spanned by a 2-D grid with a node spacing smaller than 0.25°-by-0.25°. Namely, the San Andreas grid has a node spacing of 0.01°-by-0.01°, and the grid for each of the other three regions has a node spacing of 0.0625°-by-0.0625°. These four regions were inherited from the latest version of the HTDP software [*Snay et al.*, 2013], which provides a horizontal velocity field for each of these four high-resolution grids to address the large horizontal velocity variations found in these four regions. TRANS4D's 3-D IGS08 velocity field for each of these four regions was obtained via bilinear interpolation of the West CONUS 3-D IGS08 velocity difference field to the region's finely spaced grid nodes and then adding these interpolated velocity differences to HTDP's 3-D IGS08 velocities at these same nodes. Because HTDP's IGS08 vertical velocity equals 0 at all locations, TRANS4D's vertical velocity field for each of these four regions simply corresponds to a subset of TRANS4D's vertical velocity field for the West CONUS region. Accordingly, the vertical velocity field in each of these four regions effectively has a spatial resolution of only 0.25°-by-0.25°.

This modeling process identified (or reidentified) some problems with HTDP's horizontal velocity field for West CONUS and the other four regions located within West CONUS' boundary, such as (1) shortcomings in the block fault geometry used with DEFNODE, (2) neglected postseismic motion associated with some earthquakes, (3) neglected magmatic activity associated with the Yellowstone hotspot and certain volcanoes, and (4) neglected motion associated with other geophysical phenomena. The resolution of these problems will require additional research.

4.2. Modeling Process Used in Alaska and West Canada

Vertical velocities in the AK&WCan region are much larger than those found in the other regions, in some cases exceeding 30 mm/yr. Thus, a purely geophysical model for its 3-D velocity field was developed to explain the majority of the vertical velocity variations. Then at those stations having stage-2 velocities, 3-D velocity differences were calculated by subtracting the 3-D velocities, produced by the geophysical model, from the stage-2 velocities. Then DYNAP-G was applied to these 3-D velocity differences to estimate 3-D velocity differences at the nodes of a 2-D grid having a spacing of 1° in latitude and 1.5° in longitude. Finally, the interpolated velocity difference field was added to the velocity field associated with the geophysical model to generate the 3-D velocity field adopted for the AK&WCan region. The described strategy relies on using the geophysical model to address much of the spatial variation occurring in the region's actual 3-D velocity field. That is, the use of DYNAP-G was needed only to capture long-wavelength features in the velocity difference field. So as not to lose the spatial resolution provided by the geophysical models, TRANS4D uses a 2-D grid, whose nodes have a 0.25° spacing in both latitude and longitude, to represent the region's velocity field. Bilinear interpolation was employed to obtain velocity differences for the nodes of the finer grid from those of the coarser grid.

The geophysical model developed for the AK&WCan region is composed of separate models to address tectonic motion, postseimic motion, and the motion associated with GIA. The tectonic motion model, by itself, is composed of (1) three tectonic block fault models similar to those developed by McCaffrey and Pearson for WCONUS and (2) an elastic slip deficit model associated with the subduction of the Pacific plate beneath the

North American plate. The three block fault models are based on the works of *Elliott et al*. [2010, 2013] and *Snay et al*. [2013]. The vertical motion for all of these block fault models are, mostly, negligible compared to other parts of the geophysical model, because the motion in these block fault models is primarily associated with strike-slip faulting. The elastic slip deficit model along the subduction zone produces substantial vertical motion. The general pattern of motion is subsidence over the shallow part of the locked region on the plate interface, paired with uplift centered above the downdip end of the locked zone [*Cohen*, 1996] given the very shallow dip of the subduction interface in Alaska. The adopted elastic slip deficit model was developed using the same approach as the one used in *Zweck et al*. [2002] and *Suito and Freymueller* [2009], with a few updates. A minor error in the former code was corrected, which had led to a small error in the depth of the plate interface surface. More significantly, the model for the plate interface was extended eastward based on the findings of *Elliott et al*. [2013]. The original plate interface model of *Zweck et al*. [2002] had truncated the subduction slab along the prominent edge in the slab's seismicity which had been thought to represent the edge of the slab. However, *Elliott et al*. [2013] demonstrated that the locked zone on the subduction interface extended well eastward of this.

The geophysical model for the AK&WCan region also includes a postseismic motion model for the *M*9.2 Prince William Sound earthquake of 1964 and another for the *M*7.9 Denali Fault earthquake of 2002. In the case of the 1964 earthquake, its postseismic motion during the past decade or so is represented simply as a constant velocity by using the model developed by *Suito and Freymueller* [2009]. This postseismic motion has, thus, been assimilated into the Alaskan interseismic velocity field. In the case of the 2002 earthquake, its associated velocity field still varies significantly as a function of time. Thus, TRANS4D treats its postseismic motion completely separate from the Alaskan interseismic velocity field, as described by *Snay et al*. [2013]. Briefly stated, both TRANS4D and HTDP estimate the crustal displacement from time t_1 to time t_2 as the sum of three quantities: (1) A constant velocity multiplied by the time difference, $t_2 - t_1$, (2) The coseismic displacements associated with all modeled earthquakes occurring between these two times, and (3) The cumulative postseismic displacements from time t_1 to time t_2 associated with certain earthquakes (thus far, TRANS4D includes an explicit postseismic motion model only for the 2002 Denali Fault earthquake).

Because of the transient postseismic motion associated with the 2002 earthquake, GPS-derived velocities were usually not computed for stations located in the area that deformed during this event; if they were computed, then these "velocities" were based on only pre-2002 data or they were not used for modeling the interseismic velocity field.

Finally, the geophysical model for the AK&WCan region also includes four separate GIA models, each of which accounts for one component of the total deglaciation signal. The most important GIA model addresses ongoing deglaciation that followed the Little Ice Age (LIA) glacial advance, which occurred roughly between 1550 A.D. and 1850 A.D. [*Larsen et al*., 2005]. The other three models address the response to the post-Last Glacial Maximum (LGM) deglaciation in Alaska, in British Columbia, and from the Laurentide ice sheet. The LGM occurred between 19,000 and 26,000 years ago [*Clark et al*., 2009]. In Canada and the United States, most of the LGM-associated ice sheets had melted more than 6000 years ago. The velocity predictions of the other three models are small, mostly less than 2 mm/yr in total, over the region covered by the AK&WCan model.

The post-LIA GIA model is based on an ice unloading model determined from *Berthier et al*. [2010] for the ice-thinning rates across the region. The extrapolation of late twentieth century rates to the full unloading history was based on *Larsen et al*. [2005], which is specific to southeastern Alaska, but no better estimates are available for other areas. The data from southeastern Alaska revealed that it was necessary to account for the time dependence of the ice-thinning rate since the late 1990s in more detail than *Larsen et al*. [2005]. Thus, separate scaling factors were estimated for the unloading rates for the 1992–2003 and the 2003–2012 time periods. These data also revealed that both periods required substantially faster overall ice loss than the late twentieth century average. For this project, the average uplift rate over 1992–2012 was adopted for the post-LIA model. The results predict significant temporal variations in velocity (at the level of a few to several mm/yr) within this 20 year time period, and various site time series confirm this. However, for this model, the long-term average was used because of uncertainties in predicting future interannual or other short-term variations in uplift rate.

The best fit Earth model has a 55 km thick elastic layer located over a 250 km thick asthenospheric layer having a viscosity of $3 \cdot 10^{-19}$ Pa s. There is a notable trade-off between the asthenospheric layer's thickness and viscosity, with a thinner asthenospheric layer requiring a lower viscosity. Below this asthenospheric layer, the VM5a viscosity model of *Peltier and Drummond* [2008] was adopted.

The three post-LGM models amount to a total effect of ~ 1–2 mm/yr or less (except perhaps within 50 km of the region's eastern boundary at 130°W). The effect of the main continental ice sheet is small because of the long distance between Alaska and the main ice lobes, and the effect of the post-LGM collapse of ice in Alaska is small because the asthenospheric viscosity is low. For the Laurentide model, the ICE-3G ice model [*Tushingham and Peltier*, 1991] was used, and the predictions of two different rheological models for Alaska (one unpublished and the other by *Sato et al*. [2012]) were averaged. For the Alaska LGM model, predictions of the University of Maine ice sheet model (L. Wheeler, personal communication, 2014) were adopted. The University of Maine model cuts off in southeastern Alaska, so it was augmented with the model of *James et al*. [2009] for the loss of ice in British Columbia. The effects of all these models amount to less than 2 mm/yr of vertical motion.

Because of some large residuals to some observed vertical velocities, the combined GIA model is considered to have some clear shortcomings in some locations, which will require significant new research to address. In southeastern Alaska the model provides a good fit to the data, although the uplift rates here are time variable due to the time-varying ice mass loss rates. In the Cook Inlet and Kenai Peninsula area, the GIA model appears to overestimate the rate of present-day uplift. The likely cause of this is the different temporal pattern of twentieth century ice loss from the Harding and Sargent ice fields on the Kenai Peninsula and surrounding glaciers, compared to southeastern Alaska. Evidence suggests that the mass loss in the Kenai area began earlier and has slowed down in recent decades, while mass loss in southeastern Alaska has accelerated. An exception to this is the Columbia Glacier in Prince William Sound, which lost little ice until ~1980 and then began an extremely rapid retreat. Thus, the scaling factors used with the *Berthier et al*. [2010] late twentieth century average rate are not quite appropriate for the Kenai Peninsula, and the model overestimates today's uplift rate.

4.3. Spatial Resolution of TRANS4D's Velocity Model

Figure 1 exhibits significant spatial variation in the density of the geodetic sites used in this study. Velocity data at these sites provide good coverage along most of the Pacific Coast, especially in the WCONUS region, the Vancouver region, and the AK&WCan region. Consequently, TRANS4D's velocity model for each of these three regions features a grid whose nodes are spaced 0.25° apart in both latitude and longitude. The grid for the Texas-Louisiana Coast region also has a 0.25° spacing among its nodes, not because the available geodetic data supports such a fine spacing but because its vertical velocity field warrants it. A node spacing of 0.25° roughly corresponds to a distance of 25 km between nodes along a meridian of longitude and a distance of 25 km times the cosine of the latitude along a parallel of latitude. Consequently, the resulting velocity model cannot properly represent a crustal velocity feature whose footprint is less than 25 km in extent.

The spatial resolution of TRANS4D's velocity model is even coarser in the East CONUS and South Canada region where the node spacing equals 0.5°, and in the Mainland Canada region where the node spacing equals 1° in latitude and 1.5° in longitude. For sure, there are some geographic areas where the available data would support a closer node spacing, for example, along the U.S. mid-Atlantic Coast and in parts of Michigan, Ohio, New York, and North Carolina. Also, for HTDP, the horizontal velocity fields for some areas within West CONUS have previously been modeled using a node spacing of 0.0625° or less [*Snay et al*., 2013] but not so for the vertical velocity fields in these areas. Thus, it is possible to improve upon the results presented in this publication, even using only the currently available geodetic data, although it would require further investigation of the noise present in the velocity field.

4.4. Dealing With Discrepant Velocity Data

In several areas, large discrepancies between stage-2 velocities and their corresponding stage-3 velocities occur. Such discrepancies occur especially in the vertical dimension because vertical velocities can vary greatly in both the spatial domain and the temporal domain. When the magnitude of a discrepancy (in any dimension) exceeded 3 times the standard deviation of its corresponding stage-2 value, then either the 3-D stage-2 velocity was removed from the input data file or the associated standard deviation was

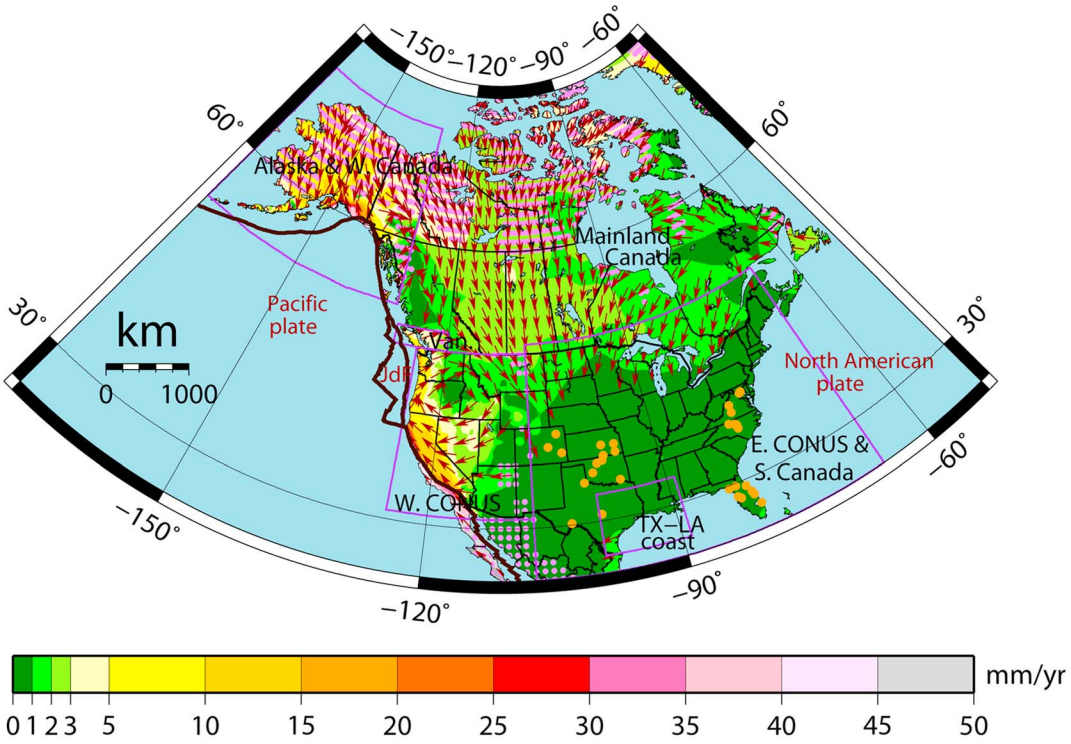

Figure 2. Estimated NA12 horizontal velocities. Contour colors indicate velocity magnitude, and dark red arrows indicate velocity direction when the velocity magnitude exceeds 1 mm/yr. Pink dots are located within areas where a velocity's north-south component and/or its east-west component have a standard deviation that exceeds 2 mm/yr. Orange dots represent the 30 GPS sites whose velocities were employed to define the NA12 reference frame. Purple line segments denote regional boundaries, and dark brown line segments denote plate boundaries.

increased in value in the input data file. Then the 3-D velocity field was reestimated by applying DYNAP-G to the revised input data file.

Large discrepancies between stage-2 vertical velocities and their corresponding stage-3 velocities were found in southern California (groundwater withdrawal), parts of coastal Texas (groundwater withdrawal), near the Yellowstone hotspot (magmatic activity), southwestern Alaska (volcanic activity), and southeastern Alaska (modern-day deglaciation). In many of these areas, sufficient geodetic data exist to produce vertical velocity models having better spatial resolution than TRANS4D's current models; however, temporal velocity variations also need to be addressed.

5. Horizontal Velocity Field

Figure 2 presents TRANS4D's horizontal velocity field relative to the NA12 reference frame that was developed by *Blewitt et al*. [2013]. The NA12 reference frame was designed to minimize horizontal velocities at locations thought to be located in the "stable" part of the North American plate. For developing this reference frame, Blewitt et al. considered only continuous GPS stations, each of whose motion is well represented by a constant velocity as indicated by the station's positional time series, at least over a data segment spanning more than 4.5 years. These authors then selected 30 of these stations, which they considered to be located in the "stable" part of the North American plate. They then used IGS08-consistent velocities, that they had estimated for these 30 stations, to estimate values for the three rotation rate parameters ($\dot{R}_x$, $\dot{R}_y$, and $\dot{R}_z$), of a seven-parameter similarity transformation, which would transform these 30 IGS08 velocities into 30 velocities whose horizontal components are minimal in value in an RMS sense. Equation (A2) of Appendix A represents such a similarity transformation. Blewitt et al. constrained the other four parameters ($\dot{T}_x$, $\dot{T}_y$, $\dot{T}_z$, and $\dot{S}$) involved in their similarity transformation to equal 0 in value. In summary, NA12 velocities are obtained by applying this similarity transformation to IGS08 velocities.

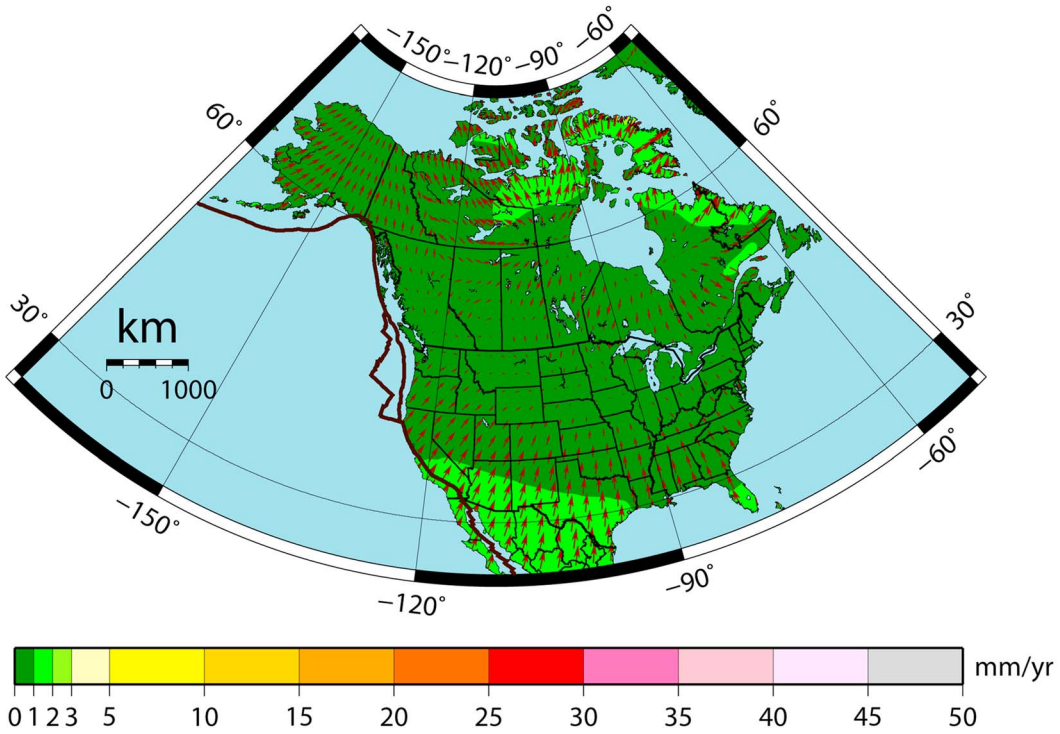

Figure 3. Present-day horizontal velocities due to the GIA associated with the past melting of the ice fields that formed during the Last Glacial Maximum. These velocities were estimated using the ICE-6G_C (VM5a) model. Contour colors indicate velocity magnitude, and dark red arrows indicate both velocity direction and magnitude.

The 30 selected stations are all located in southeastern CONUS. They are located to the east of longitude 104.6°W to avoid the crustal deformation associated with the Basin and Range Province and the Rio Grande Rift [e.g., *Kreemer et al*., 2010; *Berglund et al*., 2012]. Also, they are located south of latitude 40.2°N to minimize the horizontal deformation associated with the GIA related to the melting of ice fields formed during the Last Glacial Maximum (LGM). Blewitt et al. report that relative to the NA12 frame, these 30 stations have an RMS velocity about zero of 0.2 mm/yr in the north-south dimension and 0.3 mm/yr in the east-west dimension, some fraction of which results from far-field GIA. In addition to the horizontal velocity variation among the 30 stations, these stations may be moving horizontally together in some systematic way due to far-field GIA. Such collective motion, if it were to exist, would bias the NA12 reference frame relative to a truly "stable" North American reference frame. Thus, GIA effects were further explored in this study.

5.1. Removing GIA-Related Motion to Locate "Stable" North America

Peltier et al. [2015] and *Argus et al*. [2014b] recently introduced the ICE-6G_C (VM5a) model that describes the LGM ice load history. Their model also provides estimates for the present-day GIA-related 3-D crustal velocities associated with the melting of the LGM ice fields. Note that most of this melting occurred more than 6000 years ago. Although their model is global in extent, Figures 3 and 4 presents its estimated GIA-related velocity fields in the horizontal and vertical dimensions, respectively, but only for the vicinity of North America. Figure 3 indicates that GIA-related horizontal motion occurs throughout much of the United States and Canada. In particular, locations in southeastern CONUS are tending to move northward on the order of 1 mm/yr. Thus, the location of "stable" North America depends on whether or not this motion is taken into full consideration. In the following, a "GIA-modified velocity" is defined as a 3-D IGS08 velocity minus the 3-D velocity (at the same location) which is generated by the ICE-6G_C(VM5a) model. Hypothetically, the collection of GIA-modified velocities are referred to a reference frame that has the same origin and scale as IGS08 velocities because the developers of the ICE-6G_C(VM5a) model used IGS08 vertical velocities at selected geodetic sites to calibrate this GIA model. The goal is to find a seven-parameter similarity transformation to a new reference frame such that the transformed GIA-modified velocities exhibit little or no horizontal motion at sites located in "stable" North America. The resulting reference frame is herein called

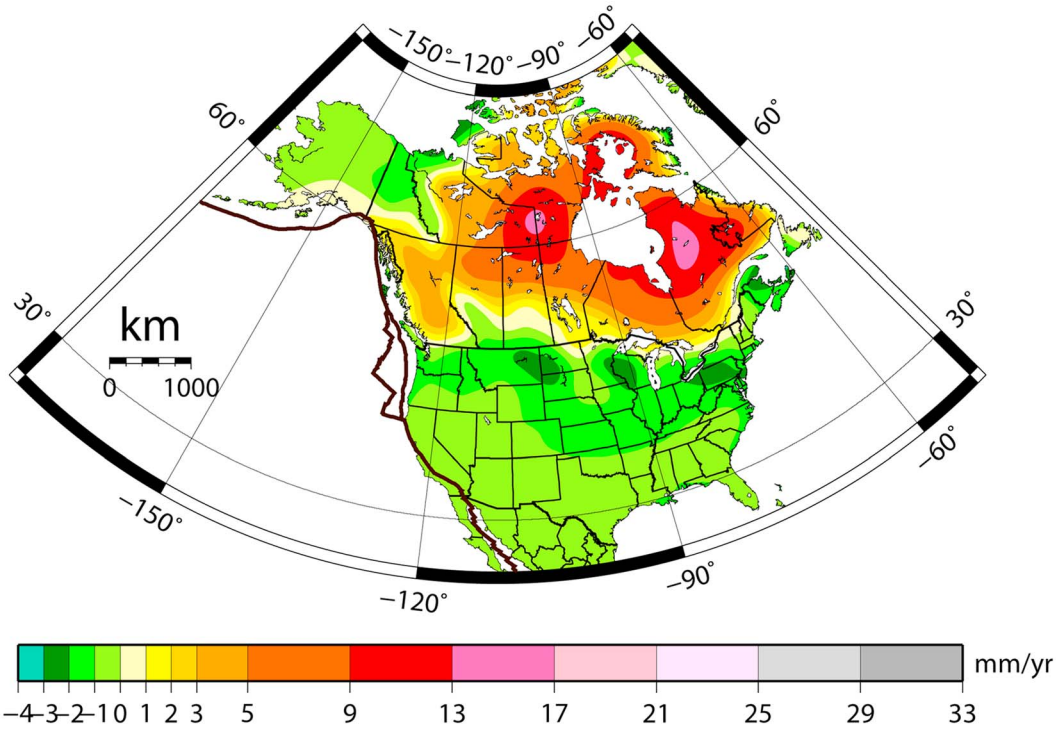

Figure 4. Present-day vertical velocities due to the GIA associated with the past melting of the ice fields that formed during the Last Glacial Maximum. These velocities were estimated using the ICE-6G_C (VM5a) model.

NA_ICE-6G. Note that this is not a reference frame appropriate for any arbitrary set of velocity vectors; it is, however, a reference frame appropriate for GIA-modified velocity vectors. Also, the concept of "stable" now refers to that part of a tectonic plate that does not experience any significant deformation other than that due to the GIA associated with the melting of the LGM ice sheets.

The search for "stable" North America started with the selection of 39 GPS sites that supposedly reside in "stable" North America and whose IGS08 velocities are well determined. Figure 5 depicts the locations of these 39 sites. The IGS08 velocities at these 39 sites were then converted to GIA-modified velocities by subtracting corresponding velocities generated by the ICE-6G_C(VM5a) model. The next step was to estimate values for the seven transformation parameters that would minimize (in an RMS sense) the horizontal components of the transformed GIA-modified velocities. Unfortunately, the 39 sites span too small of a geographic area to robustly estimate the three translation rates ($\dot{T}_x$, $\dot{T}_y$, and $\dot{T}_z$) and the differential scale rate ($\dot{S}$). Thus, seven transformation parameters for each of five additional tectonic plates (Antarctica, Australia, Eurasia, Pacific, and South America) were also estimated simultaneously with the seven transformation parameters for the North American plate, with the condition that each of the three translation rates and the differential scale rate share the same value for each of the six tectonic plates. Also, GIA-modified 3-D velocities for sites considered to be located in the "stable" parts of these five additional tectonic plates were included in the estimation process. In total, the least squares process employed GIA-modified 3-D velocities at 157 geodetic sites on six tectonic plates to estimate values for 22 transformation parameters (three rotation rates for each of six plates, plus three translation rates and one differential scale rate). These 157 sites form a subset of those employed by *Altamimi et al.* [2012] to develop a plate motion model for ITRF2008.

The GIA-modified velocity at each of the 157 sites gives rise to three observation equations, one for each velocity component (north, east, and up). The observation equation for each velocity component was assigned a weight w in accordance with the equation

$$w = \left(\sigma_1{}^2 + \sigma_2{}^2\right)^{-1} \tag{1}$$

where σ_1 equals the standard deviation of the corresponding component of the stage-2 IGS08 velocity and σ_2 equals an empirically determined value approximating a standard deviation that characterizes the

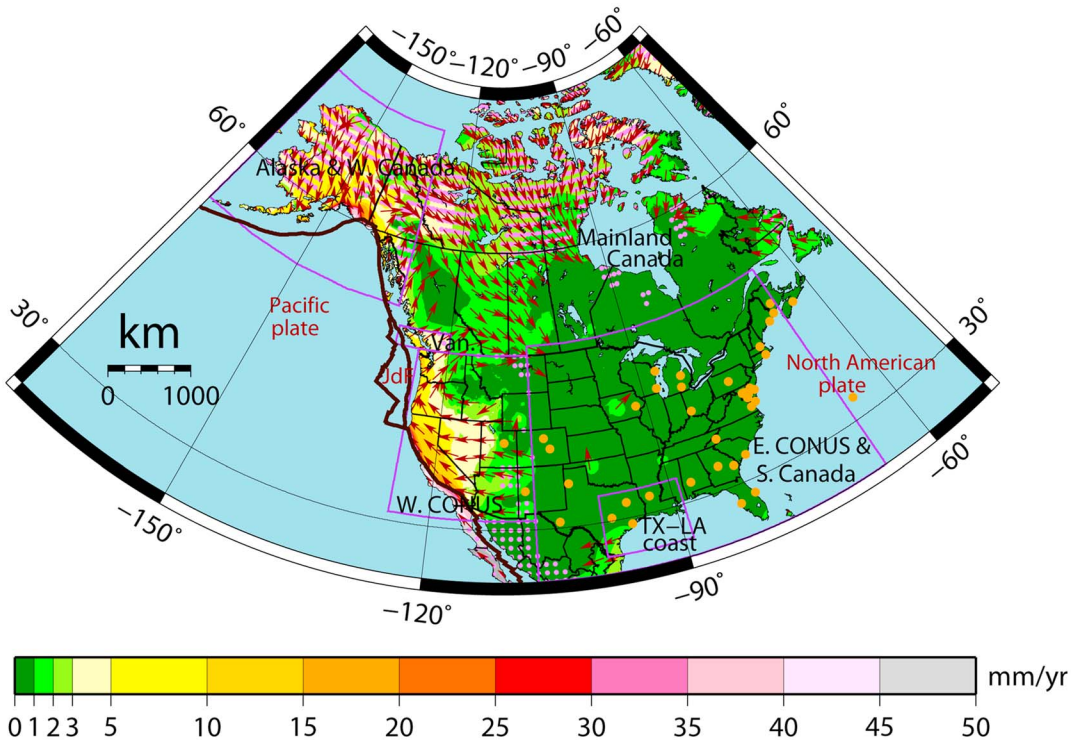

Figure 5. NA_ICE-6G horizontal velocities obtained by transforming IGS08 velocities after subtracting post-LGM-GIA-related velocities from them. Contour colors indicate velocity magnitude, and dark red arrows indicate velocity direction when the velocity magnitude exceeds 1 mm/yr. Pink dots are located within areas where a velocity's north-south component and/or its east-west component have a standard deviation that exceeds 2 mm/yr. Orange dots represent the 39 GPS sites whose velocities were employed to define the NA_ICE-6G reference frame. Purple line segments denote regional boundaries, and dark brown line segments denote plate boundaries.

uncertainty associated with both the GIA-modeled velocities and any other non-GIA motion occurring at the corresponding geodetic site. Values for σ_2 were obtained iteratively. First, two initial values for σ_2 were adopted: one denoted σ_{h0} for use with each horizontal velocity component, and another denoted σ_{u0} for use with the vertical velocity component. Then a preliminary solution to the least squares equations was calculated by minimizing the quantity

$$Q = \sum_{i=1}^{157} \left(w_{n,i} \cdot v_{n,i}^2 + w_{e,i} \cdot v_{e,i}^2 + w_{u,i} \cdot v_{u,i}^2 \right) \tag{2}$$

where ($v_{n,i}$, $v_{e,i}$, $v_{u,i}$) denote the north, east, and up components (respectively) of site i's transformed velocity relative to the "stable" part of its corresponding tectonic plate and where ($w_{n,i}$, $w_{e,i}$, $w_{u,i}$) denote the assigned weights to the corresponding observation equations.

Updated values for σ_2, denoted σ_h and σ_u, were then computed via the equations

$$\sigma_h = \sigma_{h0} \cdot \left\{ \left[\sum_{i=1}^{157} \left(w_{n,i} \cdot v_{n,i}^2 + w_{e,i} \cdot v_{e,i}^2 \right) \right] / [2 \cdot 157 - 18] \right\}^{0.5} \tag{3}$$

$$\sigma_u = \sigma_{u0} \cdot \left\{ \left[\sum_{i=1}^{157} \left(w_{u,i} \cdot v_{u,i}^2 \right) \right] / [157 - 4] \right\}^{0.5} \tag{4}$$

The denominator in equation (3) approximates the degrees of freedom involved in solving for the 18 rotation rates; the denominator in equation (4) approximates the degrees of freedom involved in solving for the three translation rates and the single differential scale rate. The resulting value for σ_h equals 0.4 mm/yr, and that for σ_u equals 0.8 mm/yr. In an overly simplistic manner, the value for σ_h may be considered to represent a nominal standard deviation for each horizontal component of the GIA velocities

Table 2. Estimated Values for the Parameters Defining Six Similarity Transformations, Each Converting GIA-Modified Velocities to Velocities Referred to the "Stable" Part of a Given Tectonic Plate[a]

Plate	Number of Sites	$\dot{R}_x$ (nrad/yr)	$\dot{R}_y$ (nrad/yr)	$\dot{R}_z$ (nrad/yr)	$\dot{T}_x$ (mm/yr)	$\dot{T}_y$ (mm/yr)	$\dot{T}_z$ (mm/yr)	$\dot{S}$ (ppb/yr)
North America	39	0.200 (0.025)	−3.310 (0.048)	−0.344 (0.040)	−0.07 (0.11)	0.20 (0.13)	−0.18 (0.12)	−0.018 (0.012)
Antarctica	7	−1.070 (0.033)	−1.502 (0.037)	3.172 (0.088)				
Australia	17	7.348 (0.042)	5.671 (0.037)	5.858 (0.035)				
Eurasia	66	−0.498 (0.030)	−2.444 (0.024)	3.708 (0.033)				
Pacific	18	−1.894 (0.036)	5.000 (0.025)	−10.595 (0.027)				
South America	10	−1.267 (0.048)	−1.519 (0.049)	−0.650 (0.037)				

[a]Values in parentheses correspond to associated standard deviations. nrad = nanoradians, ppb = parts per billion.

generated using the ICE-6G_C (VM5a) model. Similarly, the value for σ_u may be considered to represent a nominal standard deviation for the vertical component of such velocities. However, both σ_h and σ_u also incorporate the uncertainty associated with the non-GIA motion occurring at the included 157 sites. For example, such non-GIA motion includes land subsidence due to groundwater withdrawal which may be occurring at any of the 157 sites. It should be noted that the estimation process actually began with 162 sites of which five were discarded (the site known as DUCK was the only discarded site located in North America) because each of the transformed velocities at these five sites had a component whose residual had an absolute value more than 3 times greater than its corresponding standard deviation. The supporting information contains a file (Data Set S2) displaying various statistics associated with the remaining 157 sites.

Table 2 presents the values for the 22 transformation parameters which were estimated using the resulting values for σ_h and σ_u. Note that none of the estimated values for the three translation rates differs significantly from 0 at the 95% confidence level. Hence, the origin of the new NA_ICE-6G reference frame is not moving significantly relative to the origin of IGS08. Also, the estimated value of the differential scale rate does not differ significantly from 0 at the 95% confidence level. Hence, the scale of NA_ICE-6G is not changing relative to the scale of IGS08. These results attest to the consistency of the model-generated GIA velocities with the IGS08 reference frame. This consistency might have been expected because the ICE-6G_C (VM5a) model had been calibrated by using GPS-derived IGS08 vertical velocities at selected geodetic sites. Nevertheless, it is reassuring to have empirical corroboration of this consistency.

Figure 5 presents the horizontal velocity field formed by GIA-modified IGS08 velocities after they have been transformed to the NA_ICE-6G reference frame using the seven transformation parameters estimated for North America. For simplicity, the velocities displayed in Figure 5 will be referred to as "NA_ICE-6G horizontal velocities". Note that these velocities may reflect (1) errors in the ICE-6G_C (VM5a) model, (2) errors in the derived stage-3 velocities, and/or (3) motion due to phenomena other than post-LGM GIA (such as tectonic-related deformation and motion associated with modern-day deglaciation).

As compared to Figure 2, Figure 5 provides a better idea as to the whereabouts of "stable" North America. As shown in Figure 5, the NA_ICE-6G horizontal velocities at locations east of longitude 104°W and south of latitude 60°N are everywhere less than 2 mm/yr, except in southern Texas. Thus, most of this area is located within the "stable" part of the North American tectonic plate, although some of it is currently deforming due to post-LGM GIA.

5.2. Horizontal Motion Outside of "Stable" North America

The NA_ICE-6G horizontal velocity field occurring within the part of Canada located to the north of latitude 60°N remains much of a mystery due to a lack of geodetic data. For the area west of longitude 104°W, its NA_ICE-6G horizontal velocities are mostly due to other phenomena as discussed in the remaining paragraphs of this section.

The area of western CONUS located near the Pacific Coast moves in response to tectonic interactions among the North American, Pacific, and Juan de Fuca plates. These three plates meet at a point known as the Mendocino Triple Junction (MTJ), which is located less than 100 km west of the California coast and slightly north of latitude 40°N. South of the MTJ, right lateral shearing between the North American plate and the Pacific plate causes NA_ICE-6G horizontal velocities in California to be northwesterly oriented in general. The boundary zone between these two plates eventually comes ashore south of the MTJ so that much of southwestern California

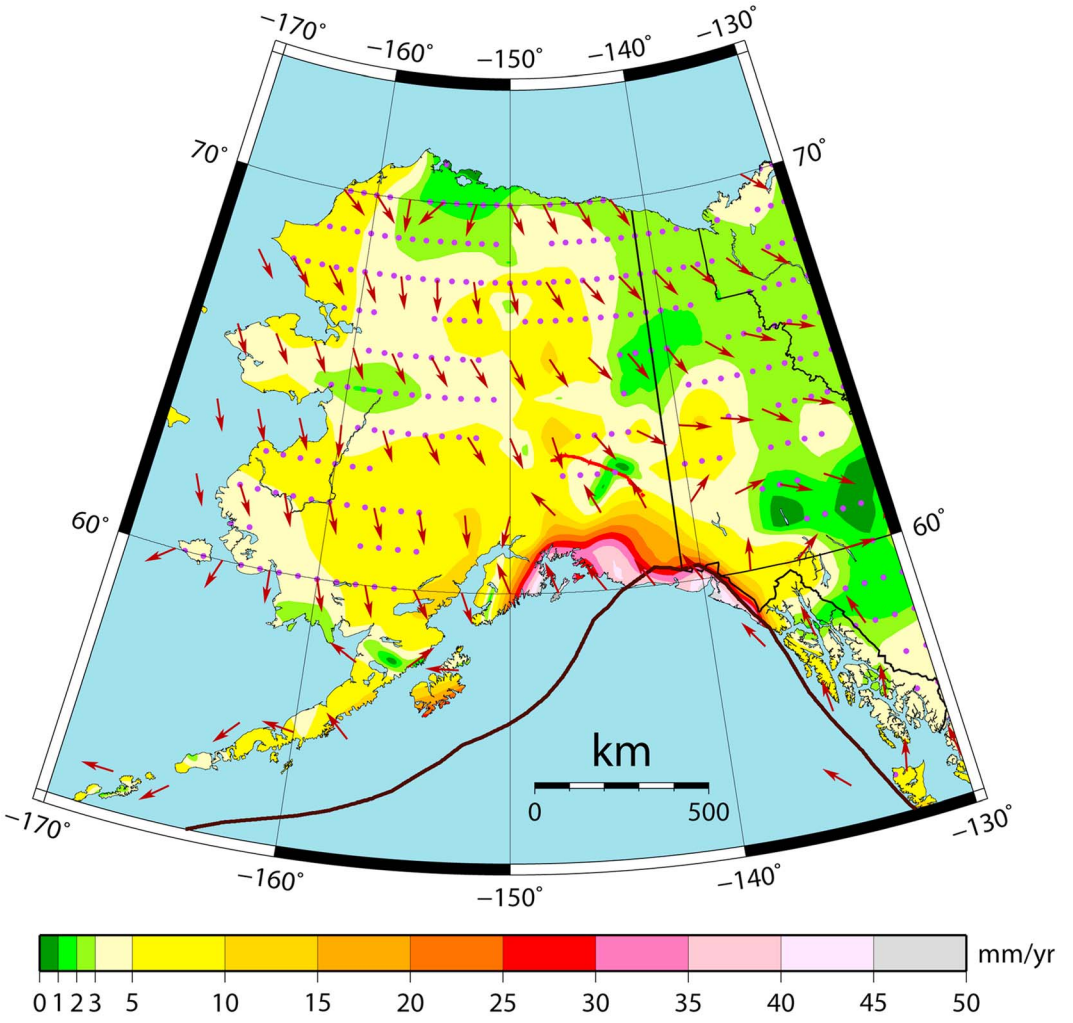

Figure 6. NA_ICE-6G horizontal velocities obtained by transforming IGS08 velocities after subtracting post-LGM-GIA-related velocities from them. Contour colors indicate velocity magnitude, and dark red arrows indicate velocity direction. Purple dots are located within areas where a velocity's north-south component and/or its east-west component have a standard deviation that exceeds 2 mm/yr. The red curve identifies the surface trace of that part of the Denali fault which ruptured during the 2002 earthquake.

resides on the Pacific plate. The largest horizontal velocity gradients in CONUS occur across the onshore part of this boundary zone which is composed of several geologic faults, the most dominant of which is the San Andreas fault. In some California areas located to the west of this boundary zone, NA_ICE-6G horizontal velocities exceed 48 mm/yr in magnitude. *Pearson and Snay* [2014] discuss the deformation occurring in southwestern CONUS in some detail.

Upon moving northward from the MTJ, NA_ICE-6G horizontal velocities gradually change orientation from northwesterly to northeasterly in a clockwise fashion. This orientation change is due to the subduction of the Juan de Fuca plate beneath the North American plate. The horizontal motion in western Oregon is essentially realized as clockwise rotation about a pole located near the Oregon-Idaho border. In Washington State, NA_ICE-6G horizontal velocities are oriented northeasterly, essentially parallel to the direction at which the Juan de Fuca plate is moving relative to the North American plate. *McCaffrey et al*. [2013] discuss the deformation occurring in northwestern CONUS in great detail.

Within the area of southwestern CONUS, which is roughly located east of California and west of longitude 110°W and south of 43°N, NA_ICE-6G horizontal velocities are oriented essentially westerly, and they grow in magnitude

from east to west. This area is undergoing east-west extension that is likely driven by gravitational collapse of the elevated continent [*Jones et al*., 1996; *Thatcher et al*., 1999; *Hammond and Thatcher*, 2005].

In Canada, as in CONUS, the largest NA_ICE-6G horizontal velocities are found along the Pacific Coast due to tectonic interactions among the North American, Pacific, and Juan de Fuca plates. These three plates meet for a second time slightly to the northwest of Vancouver Island. To the south of this triple junction, NA_ICE-6G horizontal velocities are oriented northeasterly due to the subduction of the Juan de Fuca plate beneath the North American plate. To the north of this triple junction, NA_ICE-6G horizontal velocities are consistent with the right lateral shearing associated with the relative motion between the Pacific plate and the North American plate. Along Canada's west coast, NA_ICE-6G velocities found north of this triple junction are less than 10 mm/yr in magnitude, because the Pacific-North American plate boundary is located offshore to the west of Canadian landmasses.

Figure 6 presents an enlargement of the part of Figure 5, which depicts NA_ICE-6G horizontal velocities for the area located in and around Alaska. According to Figure 6, much of Alaska's west coast is moving southeasterly at a rate of more than 3 mm/yr relative to the "stable" part of the North American plate. *Cross and Freymueller* [2008] provide evidence supporting the existence of a tectonic plate that these authors call the Bering plate. This hypothesized plate encompasses the Bering Sea, western Alaska, and the Aleutian Islands. Unfortunately, insufficient geodetic data exist in this part of Alaska to determine the exact location of the boundary between the Bering plate and the North American plate. Therefore, the horizontal velocities found in and around western Alaska may be occurring on the Bering plate or on that part of the North American plate, which is deforming as a result of its interaction with the Bering plate.

According to Figure 6, NA_ICE-6G horizontal velocities along a large extent of the northwest coast of Cook Inlet exceed 10 mm/yr in magnitude, and these velocities are oriented almost directly toward the trench that forms the interface between the Pacific plate and the North American plate. According to *Suito and Freymueller* [2009], this feature of the present-day velocity field is associated with postseismic relaxation following the *M*9.2 Prince William Sound earthquake of 1964, in particular, the relaxation that is occurring in the viscous mantle that resides in the wedge existing above the subducting Pacific plate and below the overriding North American plate. These rather large trenchward velocities provide evidence that significant postseismic deformation associated with the 1964 earthquake is continuing even 50 years after the earthquake.

The horizontal velocity field found near Alaska's Pacific coast and to the east of longitude 155°W has been discussed in great detail by *Suito and Freymueller* [2009], *Elliott et al*. [2010], *Elliott et al*. [2013], and *Marechal et al*. [2015]. The horizontal velocity field found near Alaska's Pacific coast and to the west of longitude 155°W is complex due to volcanic and seismic activities [*Cross and Freymueller*, 2008; *Gong et al*., 2015]. The horizontal velocity field occurring in northeastern Alaska remains uncertain due to a lack of geodetic data and to ongoing postseismic motion associated with the *M*7.9 Denali Fault earthquake of 2002.

6. Vertical Velocity Field

Figure 7 presents a contour map of TRANS4D's IGS08 vertical crustal velocity field for CONUS and most of Alaska and Canada. The fact that this velocity field is referred to IGS08 implies that these velocities approximate motion relative to Earth's center of mass. However, it is possible that IGS08 velocities may include a 3-D velocity bias having a magnitude on the order of 0.5 mm/yr relative to the Earth's center of mass. Thus, in this report, a location is considered to be "uplifting" only if its estimated IGS08 vertical velocity exceeds 1.0 mm/yr, and a location is considered to be "subsiding" only if its estimated IGS08 vertical velocity is less than −1.0 mm/yr. Vertical velocity differences between locations separated by less than a few hundred kilometers can, however, be considered to be more accurate, because the aforementioned velocity bias will essentially cancel out within such distances.

The most widespread feature of the estimated vertical velocity field corresponds to post-LGM GIA. This assertion may be deduced by comparing the vertical velocities depicted in Figure 7 with those depicted in Figure 4. Recall that Figure 4 displays the present-day vertical velocity field produced by the ICE-6G_C (VM5a) model. This GIA-related motion is associated with uplift across most of Canada and subsidence across much of north central CONUS. Figure 8 presents the residual vertical velocities that were computed by subtracting the vertical velocities depicted in Figure 4 from their corresponding vertical velocities depicted in Figure 7. These residual vertical velocities may be due to (1) errors in the ICE-6G_C (VM5a) model, (2) errors in the derived stage-3 velocities,

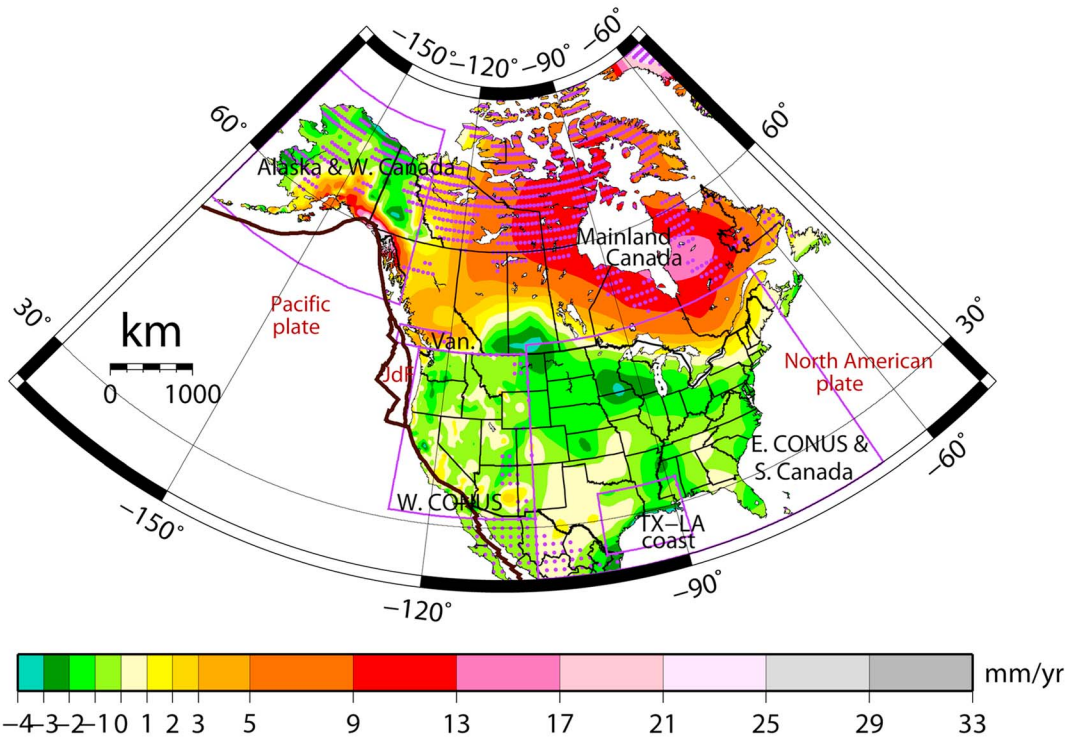

Figure 7. Estimated IGS08 vertical velocities. Purple dots are located within areas where vertical velocities have standard deviations exceeding 2 mm/yr. Purple line segments denote regional boundaries, and dark brown line segments denote plate boundaries.

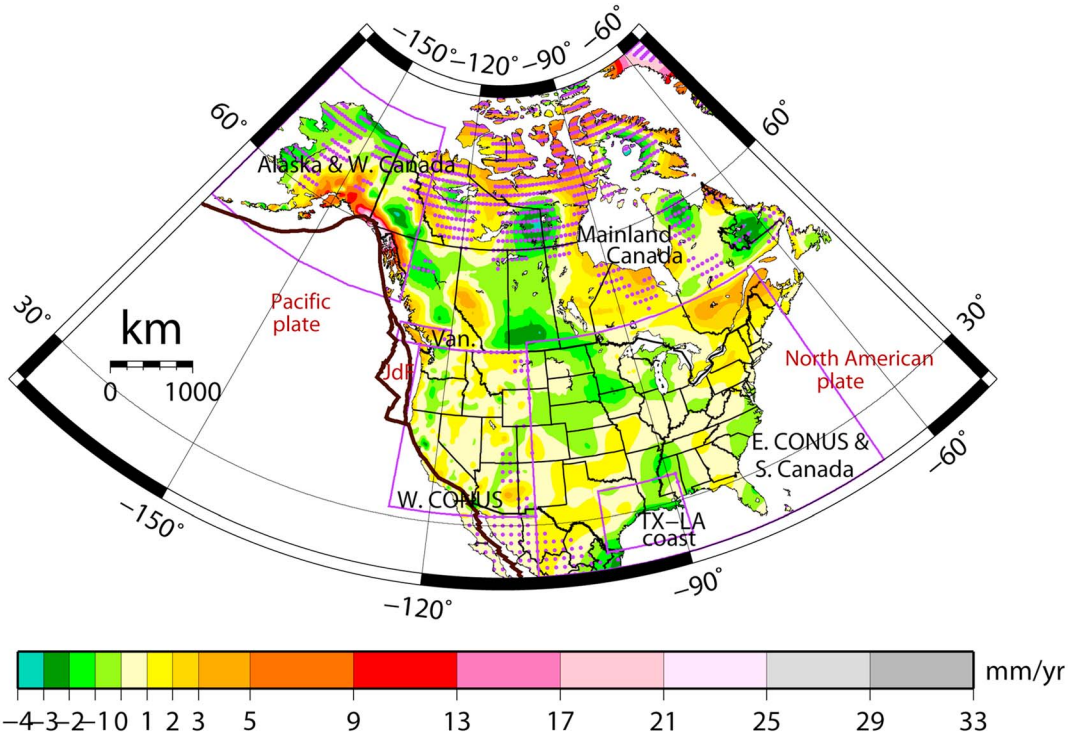

Figure 8. Residual vertical velocities obtained by subtracting post-LGM-GIA-related velocities from estimated IGS08 velocities. Purple dots are located within areas where vertical velocities have standard deviations exceeding 2 mm/yr. Purple line segments denote regional boundaries, and dark brown line segments denote plate boundaries.

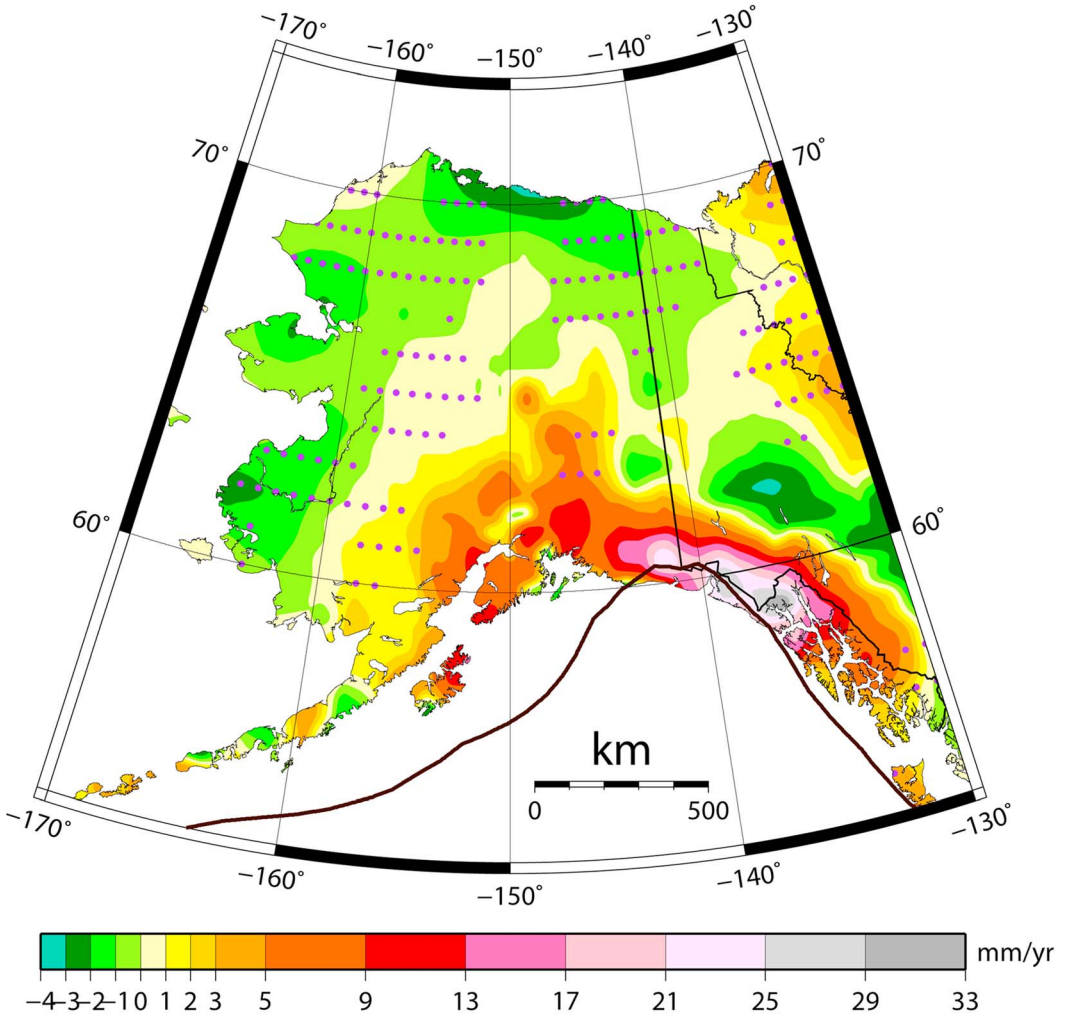

Figure 9. Residual vertical velocities obtained by subtracting post-LGM-GIA-related velocities from estimated IGS08 velocities. Purple dots are located within areas where vertical velocities have standard deviations exceeding 2 mm/yr. Dark brown line segments denote plate boundaries.

and/or (3) motion due to phenomena other than post-LGM GIA (such as the land subsidence associated with groundwater withdrawal and/or the GIA associated with modern-day deglaciation).

Some areas of pronounced residual vertical velocities are addressed in the following few paragraphs.

The largest residual vertical velocities occur in southeastern Alaska where residual uplift rates on the order of 30 mm/yr are found (see Figure 9). As mentioned previously, uplift rates in this area are associated with ongoing deglaciation following the Little Ice Age glacial advance [*Larsen et al*., 2005]. Large discrepancies between stage-2 vertical velocities and their corresponding stage-3 vertical velocities also occur in southeastern Alaska, because the actual uplift rates vary greatly in both the spatial domain and the temporal domain. As indicated in Figure 1, the existing data density across southeastern Alaska is excellent. Hence, in future studies, velocity models with finer spatial resolution can be developed for this area, but a different approach would be needed to address the temporal velocity variations found in southeastern Alaska.

Figure 8 displays three other areas of significant spatial extent where vertical velocity residuals exceed 3 mm/yr in magnitude and where adequate geodetic data are available: (1) Vancouver Island, (2) Labrador and the mouth of the St. Lawrence River, and (3) western Alberta (residual subsidence in southern Saskatchewan exceeds 2 mm/yr). The uplift found in and around Vancouver Island is associated with the subduction of the Juan de Fuca plate beneath the North American plate. The latter two regions show similar

characteristics in the 3-D residuals. Both regions have nearby paired regions of positive and negative vertical velocity residuals, with NA_ICE-6G horizontal velocities being small over the region of residual uplift and on the order of 2 mm/yr over the region of residual subsidence. The NA_ICE-6G horizontal velocities point roughly toward the region of residual subsidence. These features may result from the ICE-6G model having misestimated the LGM ice load history in these areas. Shifting some of the ice load laterally could explain these residual features; for example, the ice load model may have underestimated the amount of ice that had existed above western Alberta while overestimating the amount over southern Saskatchewan. Note that *Peltier et al*. [2015] previously identified large vertical velocity residuals occurring in western Alberta and southern Saskatchewan as indicated by profiles JJ′ and HH′ which appear in Figures 4 and 5 of their paper.

Figure 8 also displays several additional areas of significant spatial extent where vertical velocity residuals exceed 3 mm/yr in magnitude. These latter areas, however, are distributed across the northern extremes of North America where adequate geodetic data are currently unavailable. In such areas, it may be constructive to supplement the available geodetically derived velocities with velocity information from the ICE-6G_C (VM5a) model to improve TRANS4D's current velocity model. This suggestion is based on the fact that several types of nongeodetic information have contributed to the development of the ICE-6G_C (VM5a) model. To illustrate how the use of ICE-6G_C (VM5a) velocities may improve future TRANS4D velocities, consider the residual vertical velocities located near latitude 62.5°N and longitude 103°W. As shown in Figure 8, this area experiences vertical velocities less than −3 mm/yr after post-LGM, GIA-related velocities have been removed. This apparent subsidence, however, is due to large post-LGM-GIA-related uplift rates in this area, as is shown in Figure 4. TRANS4D's velocity model did not capture the effect of this GIA-related uplift because geodetically derived velocities are lacking in this area. The existence of this GIA-related uplift, nevertheless, has been independently corroborated via gravity observations obtained using the satellites of NASA's Gravity Recovery and Climate Experiment (GRACE) mission [see *Peltier et al*., 2015, Figure 6].

Another limitation of TRANS4D's velocity model is that the derived vertical velocity at a geodetic station roughly corresponds to the vertical velocity occurring at the depth to which the station is anchored. Thus, in southern Louisiana, for example, where many continuously monitored GPS stations are located on structures that are anchored 10 m or more beneath Earth's surface, a GPS-derived vertical velocity may differ significantly from its corresponding surface velocity because of differential compaction within shallow subsurface material, sediment loading, and/or erosion. As a result, significant differences exist between TRANS4D's residual vertical velocity field for Louisiana and that reported by *Shinkle and Dokka* [2004], who primarily employed leveling observations involving both shallowly and deeply anchored geodetic stations. TRANS4D's residual vertical velocity field in Louisiana agrees better with that reported by *Dokka et al*. [2006] because both studies are based on data from deeply anchored continuous GPS stations only. In their study, *Dokka et al*. [2006] attribute part of the subsidence, observed in southern Louisiana, to slip on normal faults that dip southward.

As previously mentioned, TRANS4D's vertical velocity model does not adequately capture ongoing subsidence pockets that occur in California and eastern Texas. These subsidence pockets result from the withdrawal of groundwater. Future TRANS4D models will need to employ grids whose internode spacing is smaller than 0.25°-by-0.25° to better characterize such subsidence. The same is true for modeling the uplift occurring near the Yellowstone hotspot, TRANS4D's model will need to employ grids whose internode spacing is smaller than 0.25°-by-0.25°.

Yet another limitation of TRANS4D's velocity model is that it overlooks periodic motion, such as that associated with hydrologic, oceanic, and/or atmospheric loading. The effect of periodic motion, however, has been mitigated somewhat in this study by using a velocity derived at a continuous GPS station only if this station's observations span at least 3 years and this station's positional time series contains no identifiable discontinuity during at least one 3 year time span and, for some of the solutions, by estimation of seasonal periodic motion terms. Note that periodic motion may bias a velocity derived from episodic observations at a station if the timing of the observations is out of phase with the periodicity of the local crustal motion. With the dominant mode of periodic motion being annual in nature, it would be best to perform repeated observational surveys at the same times each year, unless the surveys are being performed specifically to study periodic crustal motion.

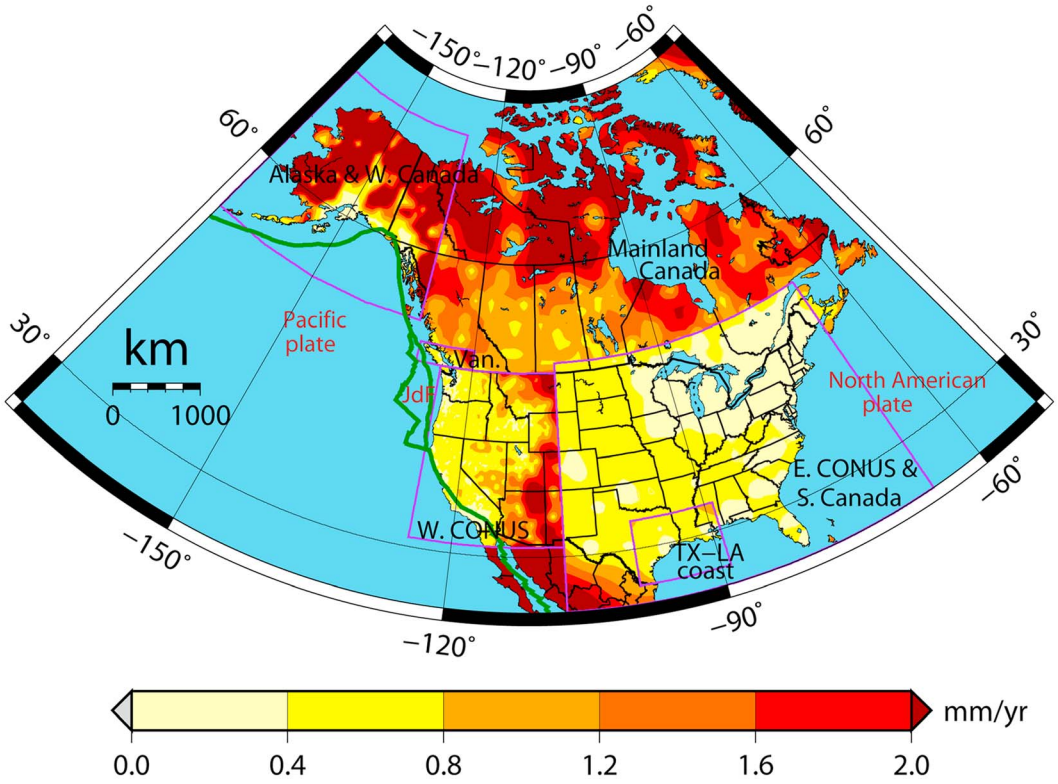

Figure 10. Standard deviations associated with estimated IGS08 horizontal velocities. The contour color denotes the greater of two standard deviations, the one associated with the corresponding velocity's north-south component and the one associated with its east-west component. Purple line segments denote regional boundaries, and dark green line segments denote plate boundaries.

7. Standard Deviations

Because the DYNAP-G software estimates 3-D velocities at the grid nodes via a rigorous least squares process, this software produces standard deviations for the three components of these estimated velocities. Standard deviations for the three components of velocities at other locations were approximated from those at the grid nodes via bilinear interpolation. Figure 10 presents the maximum of the north-south standard deviation and the east-west standard deviation for the horizontal velocity field presented in Figure 2. Large standard deviations, occurring north of latitude 60°N and in Mexico south of latitude 31°N, reflect the sparseness of GPS-derived velocities throughout these two areas. Abrupt spatial changes among estimated standard deviations often occur across regional boundaries. In particular, a drastic change occurs across the boundary between the West CONUS region (where the node spacing equals 0.25°) and the East CONUS and South Canada (ECoSCan) region (where the node spacing equals 0.5°). In the vicinity of this boundary, the density of GPS-derived velocities is similar for both regions, but in West CONUS, its data are being applied to estimate velocities at 4 times as many nodes per unit of area than is the case for ECoSCan. Hence, standard deviations are higher on the immediate west side of this boundary.

Another factor also comes into play in determining standard deviations. The DYNAP-G estimation process includes three quasi-observations at each grid node, one for each spatial dimension—north, east, and up. These quasi-observations cause the 3-D velocity vector at a node to approximate the mean of the 3-D velocities occurring at the eight neighboring nodes. The inclusion of these quasi-observations is required to estimate velocities at those grid nodes located where there are few or no geodetically derived velocities. These quasi-observations also serve to spatially smooth the estimated velocity field. In each region, these quasi-observations tend to be weighted in inverse proportion to the spatial variation of the velocity field throughout that region. Thus, the quasi-observations for ECoSCan are weighted more heavily than those for West CONUS, because velocities in ECoSCan exhibit less spatial variation than those in West CONUS.

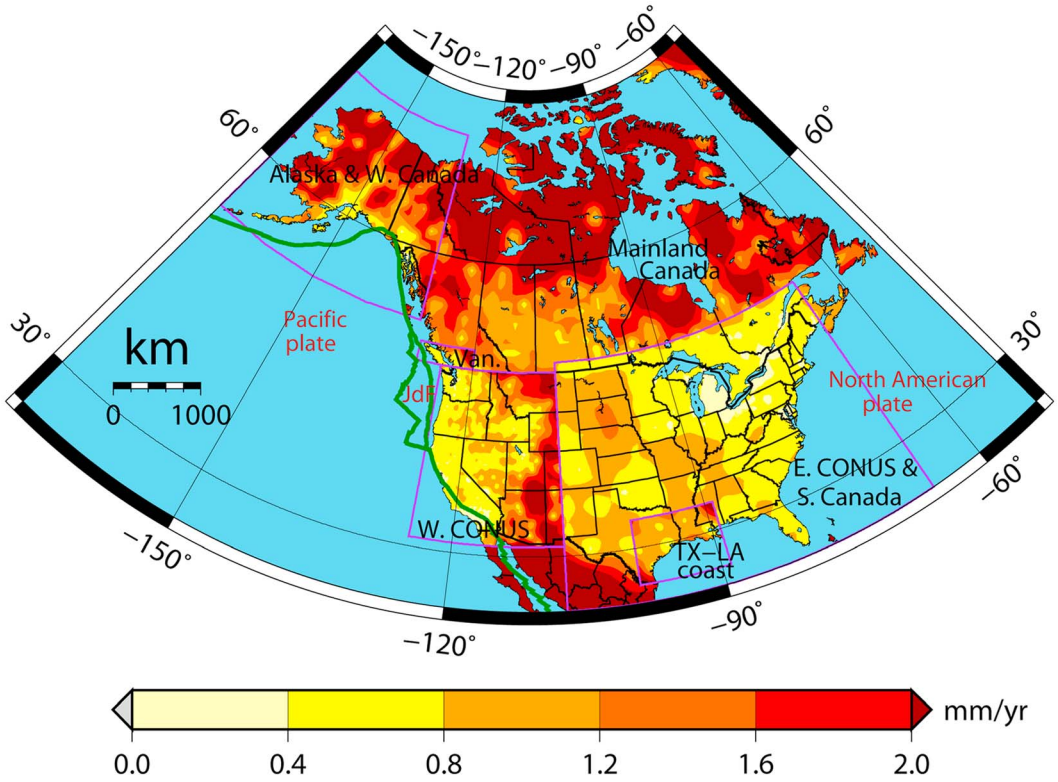

Figure 11. Standard deviations associated with estimated IGS08 vertical velocities. Purple line segments denote regional boundaries. Dark green line segments denote plate boundaries.

Accordingly, if ECoSCan and West CONUS were to share the same node spacing, standard deviations in ECoSCan would generally be lower than they would be in West CONUS in areas where these two regions have similar data densities. Differences in the standard deviations across the boundary between Mainland Canada and ECoSCan reflect the effect of the weights applied to their respective quasi-observations. In the vicinity of this boundary, standard deviations are generally higher in Mainland Canada than they are in ECoSCan, because the horizontal velocity field exhibits greater spatial variation throughout Mainland Canada than it does throughout ECoSCan. In the vicinity of their common boundary, standard deviations are generally higher in Mainland Canada than they are in ECoSCan even though there are 6 times more nodes per unit of area in ECoSCan than there are in Mainland Canada.

Figure 11 presents standard deviations for the vertical velocity field shown in Figure 7. The standard deviation of a vertical velocity is generally greater than that of either of its corresponding horizontal velocity components. In other respects, Figures 10 and 11 exhibit similar spatial patterns.

8. Summary

A numerical model for 3-D crustal velocities as a function of latitude and longitude has been developed for CONUS and parts of Alaska and Canada. This model forms the foundation for a prototype of the TRANS4D software. TRANS4D is being developed to enable geospatial professionals and others to transform 3-D positional coordinates across time and between spatial reference frames. TRANS4D represents a significant upgrade to the HTDP software that addresses only the horizontal crustal motion occurring in CONUS and parts of Alaska.

The velocity model for TRANS4D was derived mostly from repeated geodetic data collected at approximately 4300 stations. Velocities at these stations were extracted from seven separate solutions, each involving some subset of the total number of stations. A quasi-least squares process was applied to obtain a unique IGS08 velocity at each station. The resulting IGS08 velocities were then used to create a separate 3-D velocity model for each of six rectangular-shaped regions. Within each of these six regions, a regularly spaced 2-D grid (in latitude and longitude) was specified, and then (using the DYNAP-G software) bilinear interpolation in reverse was applied to the

IGS08 velocities at the stations to estimate IGS08 velocities at the grid nodes. For two of the six regions—the West CONUS region and the Alaska and West Canada region—an extra step needed to be performed because of large spatial variations in their respective velocity fields due to slip on active geologic faults. For each of these two regions, a preliminary velocity model (which accounted for fault slip and/or GIA using geophysical models) was employed to remove most of the motion associated with these two phenomena. The DYNAP-G interpolation process was then applied to the residual velocities at the geodetic stations to estimate residual velocities at the specified grid nodes. The estimated residual velocity at each grid node was then added to the corresponding velocity provided by the preliminary model to estimate the total velocity at this grid node.

The composite model formed by combining the six regional models reveals several macroscopic features of the 3-D velocity field. To better comprehend the modeled horizontal velocities, they were first modified to remove from them the present-day motion due to post-LGM GIA in accordance with the ICE-6G_C(VM5a) model. The GIA-modified velocities were then transformed to the newly introduced NA_ICE-6G reference frame that was created so as to minimize the horizontal motion of the transformed GIA-modified velocities at 39 sites that were considered to reside within the "stable" part of the North American plate. Relative to this reference frame, transformed GIA-modified velocities are less than 2 mm/yr in magnitude everywhere east of longitude 104°W and south of latitude 60°S, except southern Texas (Figure 5). Transformed GIA-modified horizontal velocities at sites located west of 104°W are mostly due to other geophysical phenomena, especially tectonics. Horizontal velocities estimated for those parts of North America which are located north of latitude 60°N mostly have large uncertainties due to a lack of geodetic data throughout much of this area.

In the vertical dimension, TRANS4D's velocity model (Figure 7) reflects the fact that the most widespread feature corresponds to the GIA associated with the past melting of ice fields formed during the LGM. This GIA-related motion is associated with uplift across most of Canada and subsidence across much of north central CONUS (Figure 4). Also in the vertical dimension, the largest uplift rates occur in southeastern Alaska, where values on the order of 30 mm/yr are found (Figure 9). The uplift occurring in southeastern Alaska is due to the GIA associated with ongoing deglaciation following the LIA glacial advance. Residual 3-D velocities near the mouth of the St. Lawrence River and in Alberta, Saskatchewan, and Labrador indicate that the ICE-6G model may have misestimated the LGM ice load history in these areas.

Figures 10 and 11 present standard deviations for the estimated horizontal and vertical velocities, respectively. The standard deviation of a horizontal velocity component is generally less than that for its corresponding vertical velocity. In other respects, Figures 10 and 11 exhibit similar spatial patterns that reflect data density, the local spacing among grid nodes, and the application of the quasi-observations that serve to prevent numerical singularities by spatially smoothing the resulting velocity field.

Appendix A: Combining Geodetically Derived Velocities From Several Solutions

Toward the objective of transforming velocities from each of the seven solutions to a single IGS08 velocity for each station, a quasi-least squares process was employed. The term "quasi" signifies that the process lacks the rigor of a true least squares process, as will be discussed shortly. The employed process is based on observation equations of the form

$$\begin{aligned}\left[V_N(j)_i, V_E(j)_i, V_U(j)_i\right]^T + \left[e_N(j)_i, e_E(j)_i, e_U(j)_i\right]^T = \left[V_N(IGS08)_i, V_E(IGS08)_i, V_U(IGS08)_i\right]^T \\ +F[x_i, y_i, z_i]\bullet\left[\dot{T}_x(j), \dot{T}_y(j), \dot{T}_z(j), \dot{R}_x(j), \dot{R}_y(j), \dot{R}_z(j), \dot{S}(j)\right]^T\end{aligned} \tag{A1}$$

Here $[V_N(j)_i, V_E(j)_i, V_U(j)_i]$ denotes the north, east, and up components of the velocity vector derived at station i in solution j, where $i = 1, 2,\ldots, 4925$ and $j = 1, 2,\ldots, 7$. Each such velocity vector is referred to the reference frame associated with solution j. Also, $[e_N(j)_i, e_E(j)_i, e_U(j)_i]$ denotes a residual vector associated with the velocity vector $[V_N(j)_i, V_E(j)_i, V_U(j)_i]$. The superscript T denotes the transpose of a vector. (Note that for any permissible value of j, solution j does not provide velocity vectors for all of the 4925 stations).

Also, $[V_N(IGS08)_i, V_E(IGS08)_i, V_U(IGS08)_i]$ denotes the north, east, and up components of the IGS08 velocity vector at station i (for $i = 1, 2,\ldots, 4925$). It is the values of these vectors that are to be estimated (together with other parameters) via the process.

Table A1. Estimated Values for the Transformation Parameters From Each Solution to the IGS Solution, Together With Other Information

Solution	IGS	NGS	NRCan	MEASURES	McCaffrey	SCEC	UAF
Total number of stations	923	1439	540	1334	989	1002	940
Number of stations in other solutions	666	1000	383	709	337	322	261
Time span of data	1994–2013	1993–2011	1994–2011	1994–2013	1993–2011	1970–2004	1992–2013
Original reference frame	IGS08	IGS08	IGS08	IGS08	SNARF 2.0	SNARF 1.0	IGS08
$\dot{T}_x$ (mm/yr)	0.00	0.05	0.03	−0.26	−0.53	0.67	−0.01
$\dot{T}_y$ (mm/yr)	0.00	0.02	0.18	0.76	−0.01	−4.67	0.05
$\dot{T}_z$ (mm/yr)	0.00	−0.03	−0.20	0.44	−2.94	−8.26	0.02
$\dot{R}_x$ (nrad/yr)	0.00	0.00	0.00	−0.12	0.54	1.61	−0.02
$\dot{R}_y$ (nrad/yr)	0.00	0.00	−0.01	−0.08	−3.09	−3.19	−0.02
$\dot{R}_z$ (nrad/yr)	0.00	−0.01	0.02	−0.08	−0.47	−0.31	−0.01
$\dot{S}$ (ppb/yr)	0.00	−0.02	0.03	0.04	0.21	0.39	−0.04

$F[x_i, y_i, z_i]$ denotes a 3-by-7 matrix whose 21 elements are each a function of the (Earth-centered, Earth-fixed) Cartesian positional coordinates $[x_i, y_i, z_i]$ of station i relative to IGS08. The values of these 21 elements are considered to be known, because the process requires only approximate values for these positional coordinates.

$\left[\dot{T}_x(j), \dot{T}_y(j), \dot{T}_z(j), \dot{R}_x(j), \dot{R}_y(j), \dot{R}_z(j), \dot{S}(j)\right]$ denotes the vector of the seven parameters that define a similarity transformation from any IGS08 velocity vector to its corresponding velocity vector referred to the reference frame of the jth solution according to the following equations:

$$\begin{aligned} V_x(j)_i &= V_x(IGS08)_i + \dot{T}_x(j) + \dot{S}(j)\cdot x_i + \dot{R}_z(j)\cdot y_i - \dot{R}_y(j)\cdot z_i \\ V_y(j)_i &= V_y(IGS08)_i + \dot{T}_y(j) - \dot{R}_z(j)\cdot x_i + \dot{S}(j)\cdot y_i + \dot{R}_x(j)\cdot z_i \\ V_z(j)_i &= V_z(IGS08)_i + \dot{T}_z(j) + \dot{R}_y(j)\cdot x_i - \dot{R}_x(j)\cdot y_i + \dot{S}(j)\cdot z_i \end{aligned} \tag{A2}$$

where $V_x(j)_i$, $V_y(j)_i$, and $V_z(j)_i$ denote the components of the velocity vector at station i relative to the reference frame of the jth solution along the x, y, and z axis, respectively; and $V_x(IGS08)_i$, $V_y(IGS08)_i$, and $V_z(IGS08)_i$ denote the components of the corresponding IGS08 velocity vector at station i along these same three axes.

For the process of obtaining a single IGS08 velocity for each station, the values for the seven transformation parameters are considered as unknowns to be estimated for each value of j. However, the "observations" represented by equation (A1) are supplemented with seven constraints that equate each of the seven parameters associated with the IGS solution to be 0 in value. Thus, the IGS solution effectively defines the IGS08 reference frame for this process. Note that values for the transformation parameters were solved for each of the other six solutions, even though four of these six solutions had already been aligned to IGS08.

The employed quasi-least squares process yields the value for the IGS08 velocity at each station i and the values for the seven transformation parameters for each solution j which minimizes the quantity

$$Q = \sum\nolimits_{j=1}^{7} Q_j \tag{A3}$$

$$\text{where } Q_j = \sum\nolimits_i Q_{ij} \tag{A4}$$

$$\text{and } Q_{ij} = \begin{cases} \left\{\left[e_N(j)_I / s_N(j)_i\right]^2 + \left[e_E(j)_I / s_E(j)_i\right]^2 + \left[e_U(j)_I / s_U(j)_i\right]^2\right\} & \text{if station } i \text{ is included in solution } j \\ = 0 & \text{if station } i \text{ is not included in solution } j \end{cases} \tag{A5}$$

Here $s_N(j)_i$, $s_E(j)_i$, and $s_U(j)_i$ are the standard deviations of $V_N(j)_i$, $V_E(j)_i$, and $V_U(j)_i$, respectively.

For the most part, the adopted values for these standard deviations agree with those reported by the institutions and/or scientists that produced the respective solutions, with the two exceptions that, for this study, (1) any reported standard deviation for a horizontal velocity component which was less than 0.1 mm/yr was reset to equal 0.1 mm/yr and (2) any reported standard deviation for a vertical velocity component which was less than 0.2 mm/yr was reset to equal 0.2 mm/yr.

The described process does not constitute a rigorous least squares process for several reasons. The most critical reason is that for any given station *i*, which is contained in at least two solutions (for example, solution *j*1 and solution *j*2); the derived velocity vector $[V_N(j1)_i, V_E(j1)_i, V_U(j1)_i]$ is statistically highly correlated with the derived velocity vector $[V_N(j2)_i, V_E(j2)_i, V_U(j2)_i]$, because these two vectors were derived from very similar sets of geodetic data. The described process treats these vectors as if they were totally uncorrelated. Hence, the term "quasi-least squares process" has been employed. Other factors that contribute to the process' lack of rigor include (a) neglected statistical correlations among the three components of any given derived velocity vector and (b) neglected statistical correlations among derived velocity vectors for the collection of stations included in any one solution.

Despite its shortcomings, the process is useful for identifying discrepant input velocities, where a discrepant input velocity corresponds to a velocity for which a component of its residual vector $[e_N(j)_i, e_E(j)_i, e_U(j)_i]$ when divided by the corresponding component of the standard deviation vector $[s_N(j)_i, s_E(j)_i, s_U(j)_i]$ has an absolute value greater than 3. When discrepant input velocities were identified, then approximately 10 of the most discrepant input velocities were either eliminated from further consideration or their corresponding standard deviations were increased. Then the process was repeated. Actually, several iterations of the process were performed, so as to refine the single IGS08 velocity estimated for each station and the resulting values estimated for the transformation parameters.

The quasi-least squares process used all 4965 derived velocity vectors from the seven solutions, even those for stations located outside the United States and Canada, so as to obtain more robust estimates for the values of the various transformation parameters. Table A1 presents the resulting estimates for the values of the transformation parameters, together with other relevant information.

Acknowledgments

The authors thank the many people and institutions that were involved in collecting and/or processing the geodetic data included in this study. The authors also thank Zuheir Altamimi, Tomás Soler, and an anonymous reviewer for suggestions that improved the presentation of this paper. This work was supported, in part, by the National Oceanic and Atmospheric Administration (DG-133C-12-SE-2355). The figures have been drawn using Generic Mapping Tools [*Wessel and Smith*, 1998]. The supporting information associated with this paper includes (a) Fortran-90 source code for Version 0.1 of the TRANS4D software (Software S1); (b) TRANS4D's *Users Guide* (Supporting Information S1); (c) stage-2 velocities for relevant geodetic sites (Data Set S1); and (d) statistics for the 157 geodetic sites involved in estimating the parameters for six transformations, each to the "stable" part of a specified tectonic plate (Data Set S2).

References

Altamimi, Z., X. Collilieux, and L. Métivier (2011), ITRF2008: An improved solution of the international terrestrial reference frame, *J. Geod.*, *85*(8), 457–473, doi:10.1007/s00190-001-0444-4.

Altamimi, Z., L. Métivier, and X. Collilieux (2012), ITRF2008 plate motion model, *J. Geophys. Res.*, *117*, B07402, doi:10.1029/2011JB008930.

Amos, C. B., P. Audet, W. C. Hammond, R. Bürgmann, I. A. Johanson, and G. Blewitt (2014), Uplift and seismicity driven by groundwater depletion in central California, *Nature*, *509*, 483–486, doi:10.1038/nature13275.

Argus, D. F., Y. Fu, and F. W. Landerer (2014a), Seasonal variation in total water storage in California inferred from GPS observations of vertical land motion, *Geophys. Res. Lett.*, *41*, 1971–1980, doi:10.1002/2014GL059570.

Argus, D. F., W. R. Peltier, R. Drummond, and A. W. Moore (2014b), The Antarctica component of postglacial rebound model ICE-6G_C (VM5a) based upon GPS positioning, exposure age dating of ice thicknesses, and relative sea level histories, *Geophys. J. Int.*, *198*(1), 537–563, doi:10.1093/gji/ggu140.

Berglund, H. T., A. F. Sheehan, M. H. Murray, M. Roy, A. R. Lowry, R. S. Nerem, and F. Blume (2012), Distributed deformation across the Rio Grande Rift, Great Plains, and Colorado Plateau, *Geology*, *40*(1), 23–26, doi:10.1130/G32418.1.

Berthier, E., E. Schiefer, G. K. C. Clarke, B. Menounos, and F. Rémy (2010), Contribution of Alaskan glaciers to sea-level rise derived from satellite imagery, *Nat. Geosci.*, *3*, 92–95, doi:10.1038/NGEO737.

Blewitt, G., et al. (2005), A stable North American reference frame (SNARF): First release, Working Group Rep., UNAVCO, Boulder, Colo. [Available at https://www.unavco.org/projects/past-projects/snarf/SNARF1.0/SNARF1.0.html, last accessed October 26, 2015.]

Blewitt, G., C. Kreemer, W. C. Hammond, and J. M. Goldfarb (2013), Terrestrial reference frame NA12 for crustal deformation studies in North America, *J. Geodyn.*, *72*, 11–24, doi:10.1016/j.jog.2013.08.004.

Bock, Y., and F. Webb (2012), MEaSUREs Solid Earth Science ESDR System, La Jolla, California and Pasadena, California USA. [Available at http://geoapp03.ucsd.edu/gridsphere/gridsphere, last accessed January 29, 2016.]

Borsa, A. A., D. C. Agnew, and D. R. Cayal (2014), Ongoing drought-induced uplift in the western United States, *Science*, *345*(6204), 1587–1590, doi:10.1126/science.1260279.

Clark, P. U., A. S. Dyke, J. D. Skakun, A. E. Carlson, J. Clark, B. Wohlfarth, J. X. Mitrovica, S. W. Hostetler, and A. M. McCabe (2009), The Last Glacial Maximum, *Science*, *325*(5941), 710–714, doi:10.1126/science.1172873.

Cohen, S. (1996), Convenient formulas for determining dip-slip fault parameters from geophysical observables, *Bull. Seismol. Soc. Am.*, *86*, 1642–1644.

Craymer, M. R., J. A. Henton, M. Piraszewski, and E. Lapelle (2011), An updated GPS velocity field for Canada, Abstract G21A-0793 presented at 2011 Fall Meeting, AGU, San Francisco, Calif., 5–9 Dec.

Cross, R. S., and J. T. Freymueller (2008), Evidence for and implications of a Bering plate based on geodetic measurements from the Aleutians and western Alaska, *J. Geophys. Res.*, *113*, B07405, doi:10.1029/2007JB005136.

Dokka, R. K., G. Sella, and T. H. Dixon (2006), Tectonic control of subsidence and southward displacement of southeast Louisiana with respect to stable North America, *Geophys. Res. Lett.*, *33*, L23308, doi:10.1029/2006GL027250.

Elliott, J. L., C. F. Larsen, J. T. Freymueller, and R. J. Motyka (2010), Tectonic block motion and glacial isostatic adjustment in southeast Alaska and adjacent Canada constrained by GPS measurements, *J. Geophys. Res.*, *115*, B09407, doi:10.1029/2009JB007139.

Elliott, J. L., J. T. Freymueller, and C. F. Larsen (2013), Active tectonics of the St. Elias orogen, Alaska, observed with GPS measurements, *J. Geophys. Res. Solid Earth*, *118*, 5625–5642, doi:10.1002/jgrb.50341.

Fu, Y., J. T. Freymueller, and T. Jensen (2012), Seasonal hydrological loading in southern Alaska observed by GPS and GRACE, *Geophys. Res. Lett.*, *39*, L15310, doi:10.1029/2012GL052453.

Fu, Y., D. F. Argus, and F. W. Landerer (2015), GPS as an independent measurement to estimate terrestrial water storage variations in Washington and Oregon, *J. Geophys. Res. Solid Earth*, *120*, 552–566, doi:10.1002/2014JB011415.
Gong, W., F. J. Meyer, C.-W. Lee, Z. Lu, and J. Freymueller (2015), Measurement and interpretation of subtle deformation signals at Unimak Island from 2003 to 2010 using weather model-assisted time series InSAR, *J. Geohys. Res. Solid Earth*, *120*, 1175–1194, doi:10.1002/2014JB011384.
Griffiths, J., J. R. Rohde, M. Cline, R. L. Dulaney, S. Hilla, W. G. Kass, J. Ray, G. Sella, R. Snay, and T. Soler (2010), Reanalysis of GPS data for a large and dense regional network tied to a global reference frame, IAG Commission 1 Symposium 2010, Reference Frames for Applications in Geosciences (REFAG2010), Marne-La-Vallee, France, October 4-8.
Hammond, W. C., and W. Thatcher (2005), Northwest Basin and Range tectonic deformation observed with the Global Positioning System, 1999–2003, *J. Geophys. Res.*, *110*, B10405, doi:10.1029/2005JB003678.
Herring, T. A., M. Craymer, G. Sella, R. Snay, G. Blewitt, D. Argus, Y. Bock, E. Calais, J. Davis, and M. Tamasiea (2008), SNARF 2.0: A regional reference frame for North America, EOS Trans. AGU, 89, Joint Assembly Suppl., Abstract G21B-01.
James, T. S., E. J. Gowan, I. Wada, and H. Wang (2009), Viscosity of the aethenosphere from glacial isostatic adjustment and subduction dynamics at the northern Cascadia subduction zone, British Columbia, Canada, *J. Geophys. Res.*, *114*, B04405, doi:10.1029/2008JB006077.
Jones, C. H., J. R. Unruh, and L. J. Sonders (1996), The role of gravitational potential energy in active deformation in the southwestern US, *Nature*, *381*, 37–41.
Kreemer, C., G. Blewitt, and R. A. Bennett (2010), Present-day motion and deformation of the Colorado Plateau, *Geophys. Res. Lett.*, *37*, L10311, doi:10.1029/2010GL043374.
Larsen, C. F., R. J. Motyka, J. T. Freymueller, K. A. Echelmeyer, and E. R. Ivins (2005), Rapid viscoelastic uplift in southeast Alaska caused by post-Little Ice Age glacial retreat, *Earth Planet. Sci. Lett.*, *237*, doi:10.1016/j.epsl.2005.06.032.
Marechal, A., S. Mazzoti, J. L. Elliott, J. T. Freymueller, and M. Schmidt (2015), Indentor-corner tectonics in the Yakutat-St. Elias collision constrained by GPS, *J. Geophys. Res. Solid Earth*, *120*, doi:10.1002/2014JB011842.
McCaffrey, R. (1995), "DEFNODE users' guide" (DEFNODE is no longer being supported). [Available at http://web.pdx.edu/~mccaf/www.defnode/, last accessed January 29, 2016.]
McCaffrey, R. (2002), Crustal block rotations and plate coupling, in *Plate Boundary Zones*, *Geodyn. Ser.*, vol. 30, edited by S. Stein and J. Freymueller, pp. 101–122 , AGU, Washington, D. C.
McCaffrey, R., R. W. King, S. J. Payne, and M. Lancaster (2013), Active tectonics of northwestern US inferred from GPS-derived surface velocities, *J. Geophys. Res. Solid Earth*, *118*, 709–723, doi:10.1029/2012JB009473.
Moritz, H. (1984), Geodetic Reference System 1980, *Bull. Géod.*, *54*(3), 388–398.
Pearson, C. F., and R. A. Snay (2014), Strain partitioning along the western margin of North America, *J. Struct. Geol.*, *64*, 67–78, doi:10.1016/j.jsg.2014.02.012.
Pearson, C. F., R. Snay, and R. McCaffrey (2014), Towards an integrated model of the interseismic velocity field along the western margin of North America, in *Earth on the Edge: Science for a Sustainable Planet*, *Int. Assoc. Geod. Symp.*, vol. 139, pp. 159–165, edited by C. Rizos and P. Willis, Springer, Berlin, Heidelberg, doi:10.10007/978-3-642-37222-3_20.
Pearson, C., and R. Snay (2007), Updating HTDP for two recent earthquakes in California, *Surv. Land Inf. Sci.*, *67*, 149–158.
Pearson, C., and R. Snay (2013), Introducing HTDP 3.1 to transform coordinates across time and spatial reference frames, *GPS Solutions*, *17*, 1–15, doi:10.1007/s10291-012-0255-y.
Pearson, C., R. McCaffrey, J. L. Elliot, and R. Snay (2010), HTDP3.0: Software for coping with coordinate changes associated with crustal motion, *J. Surv. Eng.*, *136*, 80–90, doi:10.1061/(ASCE)SU.1943-5428.0000013.
Peltier, W. R., and R. Drummond (2008), Rheological stratification of the lithosphere: A direct inference based upon the geodetically observed pattern of the glacial isostatic adjustment of the North American continent, *Geophys. Res. Lett.*, *35*, L16314, doi:10.1029/2008GL034586.
Peltier, W. R., D. F. Argus, and R. Drummond (2015), Space geodesy constrains ice age terminal deglaciation: The global ICE-6G_C (VM5a) model, *J. Geophys. Res. Solid Earth*, *120*, 450–487, doi:10.1002/2014JB011176.
Rebischung, P., J. Griffiths, J. Ray, R. Schmid, X. Collilieux, and B. Garayt (2012), IGS08: The IGS realization of ITRF2008, *GPS Solutions*, *16*, 483–494, doi:10.1007/s10291-011-0242-2.
Sato, T., S. Miura, W. Sun, T. Sugano, J. T. Freymueller, C. F. Larsen, Y. Ohta, H. Fujimoto, D. Inazu, and R. J. Motyka (2012), Gravity and uplift rates observed on southeast Alaska and their comparison with GIA model predictions, *J. Geophys. Res.*, *177*, B01401, doi:10.1029/2011JB008485.
Shen, Z.-K., R. W. King, D. C. Agnew, M. Wang, T. A. Herring, D. Dong, and P. Fang (2011), A unified analysis of crustal motion in Southern California, 1970–2004: The SCEC crustal motion map, *J. Geophys. Res.*, *116*, B11402, doi:10.1029/2011JB008549.
Shinkle, K. D., and R. K. Dokka (2004), Rates of vertical displacement at benchmarks in the lower Mississippi Valley and the northern Gulf Coast, NOAA Tech. Rep. NOS/NGS 50, Silver Spring, Md. [Available at www.ngs.noaa.gov/heightmod/NOAANOSNGSTR50.pdf, last accessed January 29, 2016.]
Snay, R. A. (1999), Using the HTDP software to transform spatial coordinates across time and between reference frames, *Surv. Land Inf. Syst.*, *59*, 15–25.
Snay, R. A., and C. Pearson (2010), Coping with tectonic motion, *Am. Surv. Mag.*, *7*(9), 28–42.
Snay, R. A., M. W. Cline, C. R. Phillip, D. D. Jackson, Y. Feng, Z.-K. Shen, and M. Lisowski (1996), Crustal velocity field near the Big Bend of California's San Andreas fault, *J. Geophys. Res.*, *101*, 3173–3185, doi:10.1029/95JB02394.
Snay, R. A., J. T. Freymueller, and C. Pearson (2013), Crustal motion models developed for version 3.2 of the Horizontal Time-Dependent Positioning utility, *J. Appl. Geod.*, *7*, 173–190, doi:10.1515/jag-2013-0005.
Suito, H., and J. T. Freymueller (2009), A viscoelastic and afterslip postseismic deformation model for the 1964 Alaska earthquake, *J. Geophys. Res.*, *114*, B11404, doi:10.1029/2008JB005954.
Thatcher, W., G. R. Foulger, B. R. Julian, J. Svarc, E. Quilty, and G. W. Bawden (1999), Present day deformation across the Basin and Range province, western United States, *Science*, *283*, 1714–1718.
Tushingham, A. M., and W. R. Peltier (1991), Ice-3G: A new global model of Late Pleistocene deglatiation based upon geophysical predictions of post-glacial sea level change, *J. Geophys. Res.*, *96*(B3), 4497–4523, doi:10.1029/90JB01583.
Wessel, P., and W. H. F. Smith (1998), New improved version of generic mapping tools released, *Eos Trans. AGU*, *79*(47), 579, doi:10.1029/98EO00426.
Zweck, C., J. T. Freymueller, and S. C. Cohen (2002), Elastic dislocation modeling of the postseismic response to the 1964 Alaska earthquake, *J. Geophys. Res.*, *107*(B4), 2064, doi:10.1029/2001JB000409.